The Astrophysical Journal Supplement Series, 190:418–448, 2010 October doi:10.1088/0067-0049/190/2/418

RESULTS OF THE LICK OBSERVATORY SUPERNOVA SEARCH FOLLOW-UP PHOTOMETRY PROGRAM: *BVRI* LIGHT CURVES OF 165 TYPE Ia SUPERNOVAE

Mohan Ganeshalingam[1], Weidong Li[1], Alexei V. Filippenko[1], Carmen Anderson[1], Griffin Foster[1], Elinor L. Gates[2], Christopher V. Griffith[1], Bryant J. Grigsby[2], Niels Joubert[1,3], Joel Leja[1], Thomas B. Lowe[2], Brent Macomber[1], Tyler Pritchard[1], Patrick Thrasher[1], and Dustin Winslow[1]

[1] Department of Astronomy, University of California, Berkeley, CA 94720-3411, USA
[2] Lick Observatory, P.O. Box 85, Mount Hamilton, CA 95140, USA
[3] Department of Computer Science, Stanford University, Stanford, CA 94305-9035, USA
Received 2009 December 13; accepted 2010 August 4; published 2010 September 30

ABSTRACT

We present *BVRI* light curves of 165 Type Ia supernovae (SNe Ia) from the Lick Observatory Supernova Search follow-up photometry program from 1998 through 2008. Our light curves are typically well sampled (cadence of 3–4 days) with an average of 21 photometry epochs. We describe our monitoring campaign and the photometry reduction pipeline that we have developed. Comparing our data set to that of Hicken et al., with which we have 69 overlapping supernovae (SNe), we find that as an ensemble the photometry is consistent, with only small overall systematic differences, although individual SNe may differ by as much as 0.1 mag, and occasionally even more. Such disagreement in specific cases can have significant implications for combining future large data sets. We present an analysis of our light curves which includes template fits of light-curve shape parameters useful for calibrating SNe Ia as distance indicators. Assuming the $B - V$ color of SNe Ia at 35 days past maximum light can be presented as the convolution of an intrinsic Gaussian component and a decaying exponential attributed to host-galaxy reddening, we derive an intrinsic scatter of $\sigma = 0.076 \pm 0.019$ mag, consistent with the Lira–Phillips law. This is the first of two papers, the second of which will present a cosmological analysis of the data presented herein.

Key words: galaxies: distances and redshifts – supernovae: general

Online-only material: extended figure, machine-readable tables

1. INTRODUCTION

The importance of supernovae (SNe) in astrophysics cannot be overstated. Having luminosities that rival those of their host galaxies, SNe can be detected out to great distances. Type Ia supernovae (SNe Ia) have been shown to be accurate cosmological distance indicators, playing a critical role in the discovery and subsequent study of the accelerating expansion of the universe and dark energy (Riess et al. 1998, 2007; Perlmutter et al. 1999; Hamuy et al. 1996a; Wood-Vasey et al. 2007; Kowalski et al. 2008; Hicken et al. 2009a); see Filippenko (2005b) for a review.

Well-sampled, high-precision light curves of nearby SNe Ia are required to better understand and calibrate SNe Ia at high redshift. Several groups have undertaken the project of collecting data sets of SN Ia light curves. The pioneering Calán/Tololo Supernova Survey acquired *BVRI* light curves of 29 SNe Ia (Hamuy et al. 1996d). The Harvard-Smithsonian Center for Astrophysics (CfA) Supernova Group has published *BVRI* light curves of 22 SNe Ia (Riess et al. 1999) and *UBVRI* light-curves of 44 SNe Ia (Jha et al. 2006b). These three data sets have proven invaluable in establishing and refining the important relationship between light-curve shape and peak luminosity that allows SNe Ia to be used as reliable distance indicators (Phillips 1993; Hamuy et al. 1996b; Riess et al. 1995, 1996; Perlmutter et al. 1997; Phillips et al. 1999). However, a larger sample of high-quality multi-color SN Ia light curves is required to further explore the luminosity–width relationship and perhaps find other nondegenerate parameters that will further improve the utility of SNe Ia as distance indicators.

The Lick Observatory Supernova Search (LOSS) follow-up program was initiated over 12 years ago with the goal of acquiring an extensive database of SN Ia photometry. This paper focuses on the results of the first 10 years of our photometric efforts using the 0.76 m Katzman Automatic Imaging Telescope (KAIT) and the 1 m Nickel telescope at Lick Observatory. Over this period, we acquired data for 165 SNe Ia with an average cadence of 3–4 days in *BVRI* for a total of 13,778 images. We also developed an automated pipeline to reduce our data to produce final calibrated magnitudes. In a forthcoming companion paper (M. Ganeshalingam et al. 2010, in preparation), we will explore the cosmological utility of our data set.

The CfA Supernova group recently released their third extensive, high-quality data set (Hicken et al. 2009b, hereafter CfA3), more than doubling the sample of published light curves of nearby SNe Ia. Their data span the years 2001–2008 and include $UBVRIr'i'$ light curves of 185 SNe Ia. While there is considerable overlap between the two data sets (69 SNe), and 17 SNe from the LOSS sample were published as part of CfA2 (Jha et al. 2006b), we contribute light curves of 79 unique SNe Ia. The Carnegie Supernova Project (CSP) has also published a set of *ugriBV* light curves of 35 SNe Ia, and a smaller subset of $YJHK_s$ light curves of 25 SNe Ia (Contreras et al. 2010). We share 14 overlapping SNe with the CSP data set.

In Section 2, we describe the mechanics behind our photometry follow-up program, including how the SNe in this paper are discovered and the resources used to observe them. In Section 3, we outline our data-reduction procedure. We address concerns of systematic errors in our reduction procedure in Section 3.5, finding that the systematic error in our data set is 0.03 mag in *BVRI* after considering a number of possible sources. We present our results in Section 4. To ensure the quality of our photometry, we do extensive comparisons to previous manual reductions of data presented here and to results for the same SNe from different telescopes. In particular, we do an in-depth comparison to the CfA2 and CfA3 data sets, finding that in general the results are consistent with small overall systematic differences with a few notable exceptions. Comparisons to the CSP data set have not been attempted because their results are given only in the natural system of the 1 m Swope telescope. Future studies of the overlap between these three data sets will be invaluable to studies of the systematics that plague SN Ia photometry from different telescopes and CCD/filter combinations. A discussion of light-curve properties from our sample is presented in Section 5, and our conclusions can be found in Section 6.

2. OBSERVATIONS

2.1. Discovery

Our photometric follow-up program is an extension of LOSS using KAIT (Li et al. 2000; Filippenko et al. 2001; Filippenko 2003, 2005a; A. V. Filippenko et al. 2010, in preparation). KAIT is a robotic telescope which is dedicated to the search and monitoring of optical transients, with a priority placed on SNe. It is based on the earlier Berkeley Automatic Imaging Telescope (Richmond et al. 1993). The search strategy is designed to optimize the capabilities of a small, lightweight telescope, finding SNe within a week of explosion. KAIT typically visits the same galaxies every 3–7 days, taking a 16–20 s unfiltered exposure which on a good night probes down to ∼19 mag (∼*R* band; Li et al. 2003a). New observations are automatically compared with archived galaxy template images. Human image checkers examine each SN candidate the next day, and the best candidates are flagged and reobserved that night. Confirmed SNe are promptly announced to the SN community through International Astronomical Union Circulars (IAUCs) and Central Bureau Electronic Telegrams (CBETs). We make an effort to spectroscopically classify and monitor newly discovered SNe with time allocated to us on the 3 m Shane telescope at Lick Observatory using the Kast double spectrograph (Miller & Stone 1993). LOSS candidates are posted publicly to encourage other SN groups to use their resources to monitor and classify the objects spectroscopically, ultimately maximizing the scientific utility of our discoveries.

Supernovae discovered by LOSS are the dominant source for LOSS photometric follow-up efforts, making up 64% of the observed sample. Our own archival images provide constraints on the rise time of new transients, allowing us to start *BVRI* monitoring soon after discovery. The remaining discoveries come mostly from the dedicated efforts of amateur astronomers such as the Puckett World Supernova Search which accounts for ∼9% of our sample.

Emphasis is placed on monitoring nearby SNe of all types that are found before maximum light, with a special effort to catch SNe Ia in the Hubble flow out to redshift $z \approx 0.05$. We try not to discriminate between SN Ia subclasses; however, our final sample of 165 most certainly suffers from observational bias and does not reflect the true demographics of SNe Ia (e.g., Li et al. 2001a, 2001b). For a discussion on the observed luminosity function from a complete SN sample, see Li et al. (2010).

Although the focus of this paper is LOSS's contribution to studies of SNe Ia, LOSS's collection of SN II-P images has been reduced using the same photometry pipeline. The SN II-P light curves and spectra have been used by Poznanski et al. (2009) to refine their use as cosmological distance indicators. A more detailed analysis of ∼60 SNe II is underway (D. Poznanski et al. 2010, in preparation) and will contain a public release of the data. In time, we will also make available our smaller data set of SN Ib/c light curves.

2.2. Telescopes

The images in our data set were acquired using the 0.76 m KAIT and the 1 m Nickel telescope, both at Lick Observatory located on Mt. Hamilton just outside of San Jose, CA. The site typically has an average seeing of ∼2″, with some seasonal dependence.

A vast majority of our observations (94%) were taken with KAIT. KAIT is completely robotic, operating only via software. Observations of an SN are initiated by creating a request file which contains the right ascension and declination of the SN along with that of a nearby guide star. For a standard observation, we expose in *B* for 6 minutes and in *VRI* for 5 minutes each, and we set a cadence of 2–3 days. The request file is sent to a master scheduler program which determines the best time to observe the field in between observations conducted for the SN search. At night, KAIT automatically observes the field without the need for any human intervention.

Time on the Nickel telescope was originally requested with the intent to calibrate SN fields against Landolt standard stars (Landolt 1983, 1992). Before 2006, the Nickel required the observer to control the telescope locally from the control room adjacent to the dome, and the major constraint on the number of nights we could obtain was the amount of time observers were able to spend driving to and from Mt. Hamilton. After 2006, the forward-thinking staff of Lick Observatory initiated a program to enable remote observing, allowing our group to observe from the University of California, Berkeley campus (and other groups from UCB and other campuses as well). To take full advantage of this, we increased the number of active Nickel observers from 1 to 5 (including many undergraduate students), and expanded our observing campaign on the Nickel to include the monitoring of more distant SNe and to complement (primarily at late times) data taken with KAIT.

KAIT has a Ritchey–Chrétien mirror set with a focal ratio of $f/8.2$. It has been outfitted with three different CCDs during the interval 1998–2008. Prior to 2001 September 11, data were taken with an Apogee back-illuminated chip having 512×512 pixels. The CCD was then changed to a newer Apogee chip with the same number of pixels though with higher quantum efficiency redward of 4000 Å. On 2007 May 12, the camera was changed once again to a Finger Lakes Instrument (FLI) camera of the same size. All three CCDs have a scale of 0$''$.8 pixel^{-1}, giving KAIT a field of view of 6$'$.7 × 6$'$.7. The CCD is thermoelectrically cooled to 60° C below ambient temperature. Standard *BVRI* broadband filters were used to obtain our images, though we switched *BVRI* filter sets on 1999 February 20. In total, we have had four combinations of CCD/filter sets on KAIT: Apogee/Old *BVRI* (KAIT1), Apogee/New *BVRI* (KAIT2), Apogee2/New *BVRI* (KAIT3), and FLI/New *BVRI* (KAIT4).

The 1 m Nickel is a Ritchey–Chrétien telescope with a primary mirror focal ratio of $f/5.3$. The CCD is a thinned, Loral, 2048×2048 pixel chip. Having a scale of 0$''$.184 pixel^{-1}, the field of view of the Nickel is 6$'$.3 × 6$'$.3. With a typical seeing of 2″, our images are oversampled; thus, in practice, we bin the pixels by a factor of two to reduce the readout time.

Normalized throughput curves for our four KAIT combinations and the Nickel telescope are compared with the standard Bessell (1990) curves in Figure 1. The throughput curves are

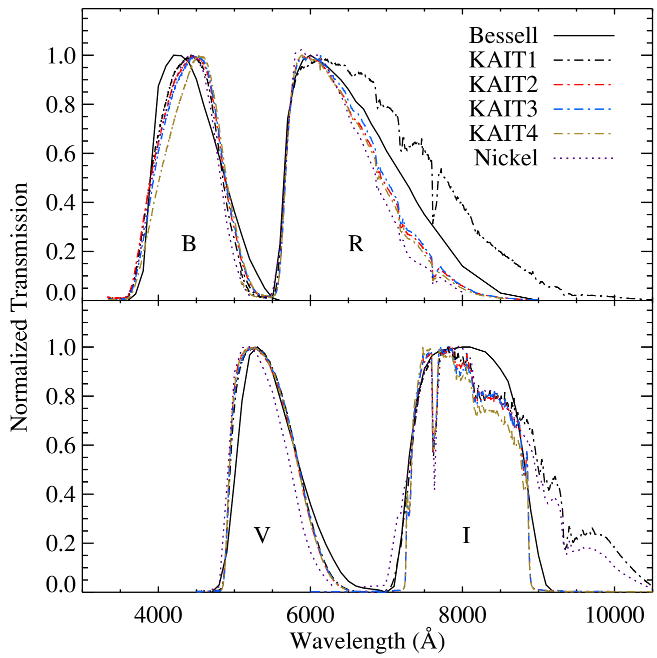

Figure 1. Transmission curve for the four different KAIT configurations and Nickel 1 m telescope compared with the standard Bessell (1990) *BVRI* curves plotted in solid black.

obtained by multiplying the transmission function of each filter by the quantum efficiency of the CCD and the atmospheric transparency at Lick Observatory. Filter transmission curves for the two different KAIT filter sets were measured in a laboratory using a Varian Cary 5000 spectrophotometer. The first Apogee CCD mounted on KAIT was also measured in a laboratory. The filter transmission for the Nickel was downloaded from the Mt. Hamilton Lick Observatory page.[4] The quantum-efficiency curves for the remaining CCDs are taken from the manufacturer's claims. In general, there is good agreement between each filter response and its corresponding Bessell curve. The largest deviations from the Bessell curves appear in the *RI* bands for the old KAIT filter set (KAIT1) and for the *I* band at the Nickel telescope. Characteristics for each photometric band can be found in Table 1.

Table 1
Characteristics of Photometric Bands

System	Filter	Central Wavelength (Å)	FWHM (Å)
KAIT1	*B*	4369	954
	V	5402	914
	R	6720	2123
	I	8191	1760
KAIT2	*B*	4364	1022
	V	5389	911
	R	6297	1249
	I	8077	1493
KAIT3	*B*	4398	971
	V	5397	921
	R	6323	1297
	I	8076	1492
KAIT4	*B*	4445	907
	V	5389	909
	R	6273	1202
	I	8061	1471
Nickel	*B*	4369	898
	V	5329	828
	R	6259	1189
	I	8125	1673

Notes. The central wavelength is defined as the wavelength between half-maximum transmission. FWHM is defined as the width between half-maximum transmission.

3. DATA REDUCTION

High-precision light curves ($\sigma_{\mathrm{mag}} \lesssim 0.03$ mag) of nearby SNe are required to properly interpret SN data collected at high redshifts to derive cosmological parameters. Imperfections in data reduction can produce systematic errors which propagate into inaccurate measurements of cosmological parameters (e.g., Boisseau & Wheeler 1991). Our data set is composed of *BVRI* images of 165 SNe with an average of 21 epochs per SN, making it impractical to manually reduce our data. Hence, we developed a software reduction pipeline that requires a minimal amount of human interaction yet provides an error-control flow system to deal with problematic data. Our reduction pipeline consists of three main processes: field calibration, galaxy subtraction, and differential photometry. Each of these will be described in the following sections.

3.1. The Calibration Pipeline

To calibrate the instrumental magnitudes of an SN to the Landolt system (Landolt 1983, 1992), the local standard stars in the SN fields need to be calibrated on photometric nights, so that differential photometry can be converted to absolute photometry. The importance of the accuracy of these photometric calibrations cannot be overlooked. As will be discussed in more detail in Section 4, one major source of the differences among published photometry for the same SNe comes from the differences in the calibrations. An error in the calibration will be directly transferred to the final photometry of an SN; thus, the goal of our calibration pipeline is to obtain reliable, self-consistent calibrations for each of the SN fields in our database.

We used both KAIT and the Nickel telescope for the calibrations of our SN fields. KAIT is a robotic telescope, so when we need to conduct calibrations on a promising photometric night, we override the automatic schedule with a manually prearranged calibration sequence. For the Nickel observations, we have a long-term project with the main goal of photometric calibration of the SNe in our photometry database. Over the years, the observations obtained with Nickel have evolved from on-site observing with a frequency of two nights per month to remote observing with a higher cadence (6–9 nights per month). In total, observations were performed over ∼50 photometric nights at KAIT and ∼100 at the Nickel telescope. Given the importance of field calibration, we try to visit fields *at least* twice and on average five times. SN 2008ar is the only SN in our sample which has just a single calibration. Calibrations for other fields from that same night are consistent with previous results, giving us confidence that the night was indeed photometric. We plan, however, to obtain more calibrations for this particular field in the future, and we will update the photometry if necessary.

For the calibration sequence on each photometric night, we arrange observations of Landolt standard stars at different airmasses throughout the night. On each photometric night, usually about 20 Landolt fields are observed at KAIT or 12–18 at the Nickel telescope. The numerous standard-star observations enable us to derive a reliable calibration solution if the night is

[4] http://mthamilton.ucolick.org/techdocs/filters/phot_filt_curves.html.

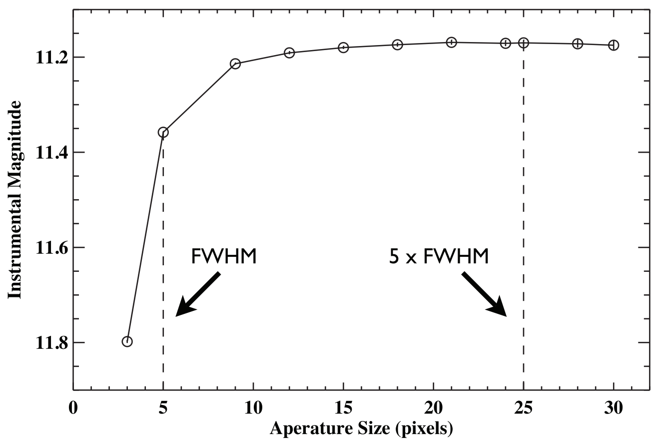

Figure 2. Instrumental magnitude of a Landolt standard star measured with aperture photometry as a function of aperture size. For this example, the FWHM of the image is approximately 5 pixels (∼1.″5). When performing absolute photometry to calibrate our SN fields, we use an aperture of 5 × FWHM of the image to sum all of the flux. As shown in this example, the instrumental magnitude asymptotically approaches its total flux value. Using an aperture radius equal to 5 × FWHM is sufficient to measure the total flux of our point sources.

photometric, and to identify a nonphotometric night when the solution shows large scatter due to clouds. Whenever possible, the SN fields are observed at an airmass that is encompassed by that of the standard-star fields (airmass usually 1.0–2.0).

It was impractical to manually reduce the very large number of photometric calibration data, so a calibration pipeline was developed. The pipeline does the following processing, with manual interactions required for some of the steps.

1. *Pre-processing of the images.* This includes removal of the bias and dark current, and flatfielding.
2. *Reduction of the standard-star observations.* First, an astrometric solution is obtained for an image to identify Landolt stars based on their location in the database. Next, aperture photometry is performed on all of the standard stars with a small, optimal aperture of radius roughly the full width at half-maximum intensity (FWHM) to increase the signal-to-noise ratio (S/N). Finally, an aperture correction is derived using the brightest (but not saturated) stars to convert the small-aperture measurement to an aperture that is large enough to include all of the flux. In a majority of cases, we find that an aperture of ∼5 × FWHM is sufficient to account for the total flux of the star as demonstrated in Figure 2. The aperture corrections are visually inspected before they are applied to all of the standard stars.
3. *Finding the photometric solution.* The instrumental magnitudes from the absolute aperture-corrected photometry and the airmasses of the standards are input to the PHOTCAL package of IRAF,[5] to solve for the extinction coefficients and color terms of the filters using equations of the form

$$b = B + C_B(B - V) + k_B X_B + \text{constant},$$
$$v = V + C_V(B - V) + k_V X_V + \text{constant},$$
$$r = R + C_R(V - R) + k_R X_R, + \text{constant, and}$$
$$i = I + C_I(V - I) + k_I X_I + \text{constant}.$$

In the above set of equations, lower-case letters represent the magnitudes in the natural system of the telescope, upper-case letters are magnitudes in the Landolt system, X_i are the airmasses of the observation, C_i are linear color terms, and k_i are extinction coefficients. We tested the inclusion of a color term proportional to airmass, but found that it did not significantly improve the scatter in the fit.
This is an interactive process. Ideally, if the night is photometric, all standard stars should be used in the solution. However, due to cosmic rays, CCD defects, or poor S/Ns for some fainter standard stars, there are often outliers in the solutions. We carefully remove the outliers in an attempt to achieve solutions with the following precisions: root-mean square (rms) < 0.04 mag for KAIT *B*, <0.03 mag for KAIT *VRI*, <0.03 mag for Nickel *B*, and <0.02 mag for Nickel *VRI*. We also check the number and source of the outliers to identify nonphotometric nights. If a relatively large fraction ($\gtrsim 15\%$) of the data points are outliers, or if all stars in a particular image are outliers (a sign of cloud cover during the exposure), the night is marked as being nonphotometric.
4. *Reduction of the SN fields.* The instrumental magnitudes of the local standard stars are first measured with a small optimal aperture. Aperture corrections are then determined from several bright stars and applied to all of the stars. The photometric solution derived from the Landolt standard stars is applied to derive the magnitudes of the local standard stars in the standard system.
5. *Combining the calibrations from different photometric nights.* For the calibrated magnitudes of a star in any band, an iterative process is invoked to remove 3σ outliers until the final average value has rms < 0.03 mag. The error of the calibrated magnitude is calculated as rms$/\sqrt{N}$, where N is the total number of calibrations used in deriving the average (following the definition of the standard deviation of the mean). An example of this process is shown in Table 2.

3.2. Galaxy Subtraction

A majority of SNe are found close to bright regions of their host galaxy, requiring galaxy subtraction to isolate the SN flux before photometry can be performed accurately. Template images of the host galaxy are obtained on a clear night during a dark run after the SN has faded beyond detection. Host-galaxy templates are visually inspected and chosen to have low background counts and an FWHM of ⩽2.″0. In cases where we had multiple high-quality templates, the images are registered and added together to produce a single deeper template.

Images are bias subtracted and twilight-sky flatfielded automatically at the telescope. Cosmic rays are removed using the `cosmicrays` procedure in the IRAF DAOPHOT package. We adopt parameters which ensure the replacement of obvious cosmic rays (objects with a small FWHM compared to the average FWHM constrained by the nights with the best seeing) with background values while not affecting objects having stellar profiles.

Data images are registered to the template image by matching congruent triangles formed by objects which have a peak intensity value that is above the background in both images. The data image is then geometrically mapped to the template image using the `geomap` routine in IRAF.

Two independent template-subtraction routines were employed with our data set, providing a consistency check for

---
[5] IRAF, the Image Reduction and Analysis Facility, is distributed by the National Optical Astronomy Observatory, which is operated by the Association of Universities for Research in Astronomy (AURA), Inc., under cooperative agreement with the National Science Foundation (NSF).

Table 2
Example of the Calibration Pipeline Output

R.A. (hr)	Decl. (deg)	B (mag)	V (mag)	R (mag)	I (mag)	Telescope
14.370000	−0.392374	17.261 X	16.687	16.295	15.868	20070616_kait
14.370002	−0.392362	17.354	16.731	16.280	15.862 X	20070617_kait
14.370001	−0.392341	17.289	16.711	16.282	15.917	20080118_kait
14.369999	−0.392355	17.291	16.679	16.263 X	15.918	20080119_kait
14.369999	−0.392362	17.367	16.725	16.342	15.954	20070609_40in
14.369999	−0.392362	17.367	16.706	16.370	15.950	20070616_40in
14.369998	−0.392348	17.350	16.708	16.345	15.945	20070617_40in
14.369999	−0.392355	17.354	16.706	16.333	15.958	20070708_40in
14.369998	−0.392345	17.427 X	16.750	16.386 X	15.927	20070805_40in
14.369999	−0.392362	17.370	16.748	16.344	15.954	20070804_40in
14.369999	−0.392341	17.265 X	16.660	16.292	15.963	20070811_40in
14.370000	−0.392328	17.357	16.736	16.359	15.963	20070812_40in
14.370001	−0.392346	17.372	16.761	16.340	15.971	20070820_40in
14.369999	−0.392326	17.359	16.528 X	16.355	16.032 X	20070821_40in
14.370002	−0.392346	17.376	16.752	16.327	15.956	20070824_40in
14.369999	−0.392333	17.375	16.731	16.337	15.901	20080112_40in
Average:						
14.369997 (15) 16	−0.392349 (05) 16	17.352 (008) 13	16.719 (008) 15	16.329 (008) 14	15.939 (008) 14	

Notes. This is for a star in the SN 2007af field, which has been observed on 16 photometric nights. The entries marked with an "X" are removed during the iterative process and are not used to calculate the final SN magnitude.

our photometry. Subtraction method 1 (SM1) is based on the ISIS package (Alard & Lupton 1998) as modified by Brian P. Schmidt for the High-z Supernova Search Team (Schmidt et al. 1998). The convolution kernel is computed as a function of position using stars in both images chosen automatically by ISIS. Ideally, the software avoids saturated stars, stars with nonstellar profiles, and cosmic rays. Our default parameters use three stamps in the x-direction and three stamps in the y-direction to determine the spatial variation in the kernel. The image with the better seeing (in most cases the template) is then convolved to match the seeing of the other image and the two images are subtracted. A 60 × 60 pixel square centered on the SN in the subtracted image is then copied onto the corresponding region in the observation image.

Subtraction method 2 (SM2) determines the convolution kernel with the IRAF task `psfmatch` (Phillips & Davis 1995) using three field stars chosen in the template image that are well above the background and are not saturated. Similar to SM1, the image with the better seeing is then convolved to the other image using the averaged kernel. Unlike SM1, which automatically finds stars to compute the kernel, SM2 uses the same three stars for all of the data images associated with a particular template. The intensity of the two images is matched using a rectangular region of 60 × 60 pixels centered on the brightest star. The images are then subtracted. As in SM1, the SN in the subtracted image is pasted back onto the observation image. An example image from our subtraction pipeline is shown in Figure 3.

As both of these subtraction methods are automated, it is inevitable that our software will produce poor subtractions for data taken under less than optimal conditions. In the worst of circumstances, such as data taken during bad weather or poor seeing conditions, we are left with no choice but to eliminate data that fail both subtraction pipelines. To minimize the number of discarded images, we have implemented an error-control system to salvage images that initially cause the subtraction pipeline to fail.

The robustness of SM1 ensures that a subtracted image will always be output, though the quality of the subtracted image may be questionable if SM1 mistakenly uses a nonstellar source to construct the kernel. The most likely candidates for stamps that produce bad subtractions are cosmic rays that elude removal and galaxy nuclei from either the host galaxy or background galaxies. In such cases, our recourse is to identify suspect images and manually choose stamps until a satisfactory subtraction is obtained. The identification of such subtractions is done by the inspection of the final light curve. Comparison of the results of SM1 to SM2 generally indicates when one subtraction method fared better than the other. In cases where SM2 produces superior results, it is usually because the stamps chosen by SM2 are set a priori while SM1 chooses stamps on the fly.

For SM2, there are two main sources of potential failures: a bad point-spread function (PSF) for the kernel and an error in the intensity transformation. In the case of a bad PSF from one of the three stars, the convolution kernel is computed using the average of the remaining two stars. In the event that all three stars prove problematic (as in a case where none of the three stars is present in the data image), the pipeline exits without producing a subtraction. If the intensity matching first fails using the brightest star of the three stars, SM2 then uses a 60 × 60 pixel square about the next-brightest star.

An analysis of our finalized photometry shows that 81% of our data uses the results from both SM1 and SM2, 18% from only SM1, and 1% from just SM2. Of the two subtraction algorithms, SM1 produced the most robust results, yielding better subtractions in instances where our galaxy template was not optimal. In most instances where SM2 gave superior subtractions, better SM1 subtractions could be produced by manually choosing stars to compute the convolution kernel.

A minority of SNe in our data set occurred far from the nucleus of the host galaxy and do not suffer from significant galaxy contamination as determined by inspection of late-time images. For these SNe, images were only registered before performing differential photometry. Table 3 contains a list of SNe which did not require galaxy subtraction, together with their offset from the host-galaxy nucleus.

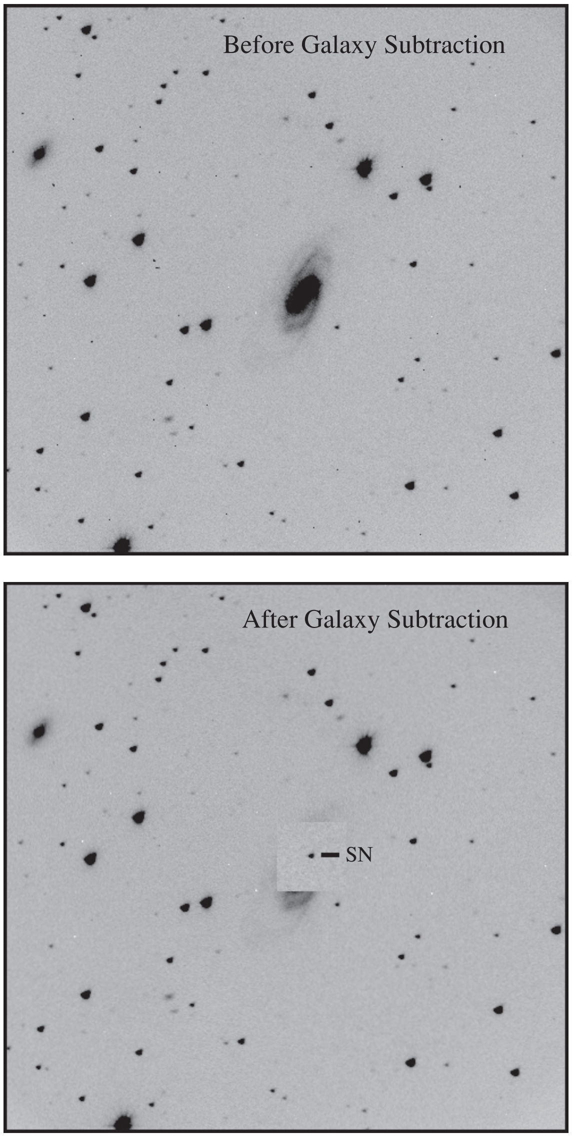

Figure 3. Example of our galaxy subtraction pipelines. The top image shows SN 2003gq on 2003 August 1 UT. The SN is embedded deep within the host galaxy. We can isolate the flux of the SN using our galaxy subtraction pipelines and paste a stamp of the subtracted image onto the data image at the position of the SN.

3.3. *Differential Photometry*

Differential photometry was performed using the PSF-fitting method in the IRAF DAOPHOT package (Stetson 1987) to measure the SN flux relative to local standards in the field. Depending on the field, three or more of the brightest stars are chosen manually to construct a model PSF. Using a fitting radius equivalent to the FWHM of each data image (usually 3–5 pixels), the PSF is modeled out to 20 pixels. Instrumental magnitudes are measured for the SN and local standards of sufficient brightness found in the calibration pipeline.

The instrumental magnitudes are transformed into the standard Landolt system using the following system of equations:

$$b = B + C_B(B - V) + \text{constant},$$
$$v = V + C_V(B - V) + \text{constant},$$
$$r = R + C_R(V - R) + \text{constant, and}$$
$$i = I + C_I(V - I) + \text{constant}.$$

Table 3
SNe Not Requiring Galaxy Subtraction

SN	East ($''$)	North ($''$)
1998de	71.9	3.4
1999gh	52	15.8
2000cx	−23	−109.3
2001ah	−4.3	−32.4
2001cj	−7.6	35.2
2003fa	−9.5	48.9
2004E	3.2	20.4
2005cf	−15.7	123
2006bt	−44.4	−22.9
2006cp	19.9	−15.3
2006em	21.4	50.9
2007fr	5.5	−33.5

Note. SN offsets from the host-galaxy nucleus are given.

In the above set, the lower-case bandpass letters on the left-hand side are instrumental magnitudes and the upper-case bandpass letters are the transformed Landolt magnitudes. The coefficients C_i represent the averaged color terms found from multiple photometric nights. The zero point and effects of atmospheric extinction are absorbed into a constant which drops out in differential photometry.

A solution to this system of equations requires instrumental magnitudes for *BVRI*. Occasionally, data for one bandpass do not exist or are of such poor quality that galaxy subtraction or PSF-fitting photometry cannot be performed with confidence. As an initial zeroth-order solution, we use the instrumental magnitude from data taken within 10 days of the absent data. As our data are well sampled, this provides an adequate solution given that there is usually not a significant change in the SN flux between the two dates. As a check on this assumption, we compare the borrowed magnitude to the magnitude derived from a third-order polynomial fit to the final light curve 10 days before and after the date of the borrowed data. Instances in which the two differ by 0.1 mag are flagged. The borrowed data are then replaced by the magnitude derived from the fit (assuming a reasonable fit is found) and the transformation equations are again solved for the color-corrected Landolt standard magnitudes. As this is a second-order correction, we find that an uncertainty of 0.1 mag for the *B* band propagates into an error of <0.01 mag for *VRI*. A summary of all of our averaged color terms can be found in Table 4.

Our goal is to perform differential photometry of the SN in comparison to those local standard stars which are sufficiently bright to be measured accurately, but do not saturate the detector, and to choose only those stars which give the most consistent results. The algorithm devised to satisfy both constraints goes as follows. The SN magnitude is calculated using all of the available local standard stars found with the calibration pipeline, an error-weighted mean is taken using the uncertainties in the calibrated magnitudes of the local standard stars (typically $\leqslant$0.02 mag), stars which give an SN magnitude more than 2.5 times the rms in the scatter of the magnitudes are removed, and the error-weighted mean is recalculated. This is done for every data image for a particular SN, giving a different set of stars for each night's data. We then take the set of stars that are present in more than 2/3 of the individual sets of stars from each night's data. Subsequently, these local standard

Table 4
Summary of Color Terms

Telescope/Filter Set	Observed Color Terms[a]				Synthetic Color Terms[b]			
	C_B	C_V	C_R	C_I	C_B	C_V	C_R	C_I
KAIT1 (Apogee/Old *BVRI*)	−0.095	0.027	−0.181	−0.071	−0.035	0.029	−0.180	−0.049
KAIT2 (Apogee/New *BVRI*)	−0.085	0.032	0.062	−0.007	−0.043	0.040	0.066	−0.005
KAIT3 (Apogee2/New *BVRI*)	−0.057	0.032	0.064	−0.001	−0.073	0.034	0.056	−0.005
KAIT4 (FLI/New *BVRI*)	−0.134	0.051	0.107	0.014	−0.124	0.039	0.078	0.000
1 m Nickel	−0.092	0.053	0.089	−0.044	−0.004	0.084	0.123	−0.029

Notes.
[a] Observed color terms are averages from observations of Landolt standards over many photometric nights.
[b] Synthetic color terms are derived from synthetic photometry of spectrophotometric standards presented by Stritzinger et al. (2005) using the instrumental response curves found by multiplying the quantum efficiency of the CCD by the filter transmission and the atmospheric seeing at the telescope site.

stars are visually inspected to ensure that they are not background galaxies and that they do not saturate the detector.

Our algorithm works well for cases in which there are many available local standards in the field, but can fail for sparse fields in which there are only two or three local standards. In such situations, the best we can do is manually choose local standards which are bright and give a consistent measurement for the SN magnitude.

The above procedure is applied to results from both SM1 and SM2. Light curves for SM1 and SM2 are visually reviewed. In cases where SM1 and SM2 both produce reliable subtractions, the mean is taken to be the final SN magnitude. If one subtraction method fared better than the other, the more reliable result was taken to be the final magnitude.

While we have chosen to provide our photometry in standard *BVRI* bands, other groups including Hicken et al. (2009b) have released their data set of comparable size in both the standard system and the natural system of their telescope. There are benefits and detriments to photometry in either system. The standard system allows photometry from different telescopes to be easily compared and combined in cases where *S*-corrections (Stritzinger et al. 2002) are small. As we are using photometry from two different telescopes and four different KAIT CCD/filter combinations, putting our photometry in a standard system is a sensible choice. However, this procedure assumes that the color terms derived from the color of our standard stars apply to the colors of an SN, which is not necessarily true as the spectral energy distribution of a standard star will differ from that of an SN. Photometry in a telescope's natural system avoids adding errors to the results from color corrections and should provide less scatter in SN flux measurements. The downside is that SN photometry from different telescopes is not readily comparable and requires accurate measurements of each telescope's transmission function. Currently, we rely on the quantum-efficiency curve supplied by the CCD manufacturer to construct our transmission curve. Although we have chosen to provide our photometry in the standard system, if there is sufficient demand for photometry in the natural system, we can make those data available.

3.4. Error Budget

Typically, we have multiple photometric observations of a given field for the purposes of calibrating the magnitude of local standards to Landolt standards. The error in the calibration of the local standard stars is taken to be the rms of N observations divided by $\sqrt{N}$ (i.e., the uncertainty in the mean). To ascertain the error in our galaxy subtraction and PSF-fitting photometry routines, artificial stars with the same magnitude and PSF as the SN were added randomly to the data and re-extracted. Fifteen artificial stars were added within 60 pixels of the SN, often placing the artificial star in a background region of similar complexity to that of the SN. Another 15 were added randomly to the rest of the data image. The scatter in the magnitudes of the 30 recovered artificial stars was taken to be the uncertainty in our galaxy subtraction and photometry pipelines.

An implicit assumption in our treatment of this uncertainty is that we trust our galaxy subtraction and calculated PSF. In cases where our galaxy-subtraction pipeline performs less than optimally and host-galaxy light is improperly subtracted, our measured SN magnitude will be inaccurate. This leads to artificial stars which do not accurately represent the profile of the SN and hence an error which does not truly represent the error in our galaxy subtraction and photometry pipelines. In such cases, we benefit from having two independent subtraction pipelines. Since both subtractions are reducing the same data image, we expect the error from our artificial-star simulations to be similar, providing us with a check on the simulation's validity.

The final error for each subtraction method is taken to be the scatter from recovering the artificial stars added in quadrature with the calibration error. When data from both subtraction methods are combined, we take the final uncertainty to be the rms in the two SN magnitude measurements added in quadrature with the quadrature addition of the error from the two subtraction pipelines, assuming the errors from the two pipelines are perfectly correlated.

3.5. Systematic Errors

A major concern for large photometric data sets is the role of systematic errors. In this section, we address possible sources of systematic errors and the possible impact such errors play on our final photometry for the LOSS data set.

3.5.1. Color Terms

The observed color terms presented in Table 4 are averages of the color terms derived from observations of Landolt standards on photometric nights. Any evolution of the color terms as a function of season or over time will produce systematic errors in the final photometry correlated with the color of the SN and comparison stars. Plotted in Figures 4 and 5 are the temporal evolution of our color terms for KAIT and the Nickel telescope, respectively. There have been no filter or CCD changes during our campaign on the Nickel, giving a large baseline to determine evolution in the color terms. We see no evidence of any significant evolution over the eight years of our observations.

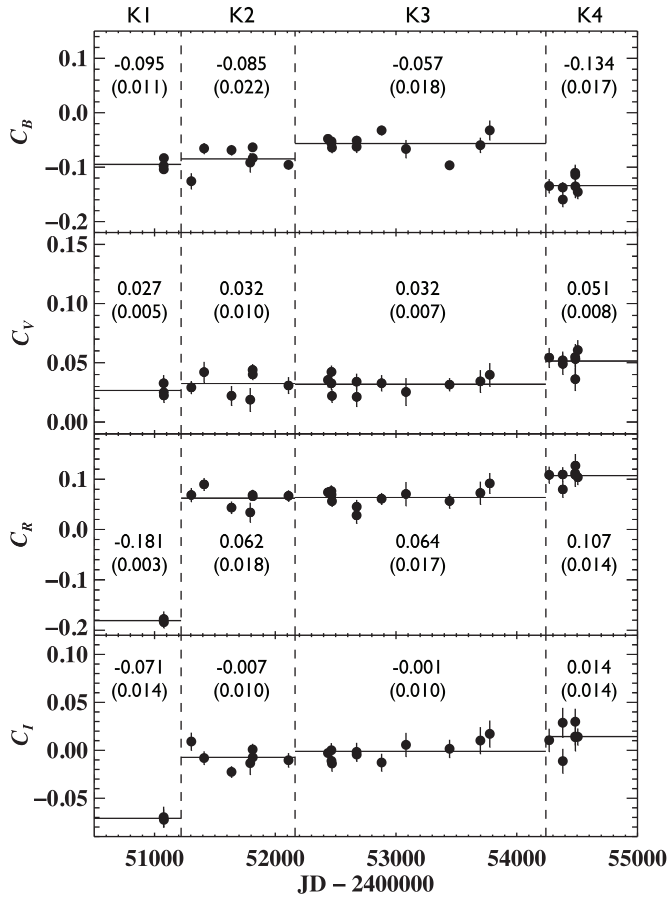

Figure 4. KAIT color terms as a function of time. The dashed vertical lines indicate changes in the CCD/filter set (K1–K4). The solid horizontal lines indicate the mean color term for each set. The mean is also indicated along with the rms in parentheses.

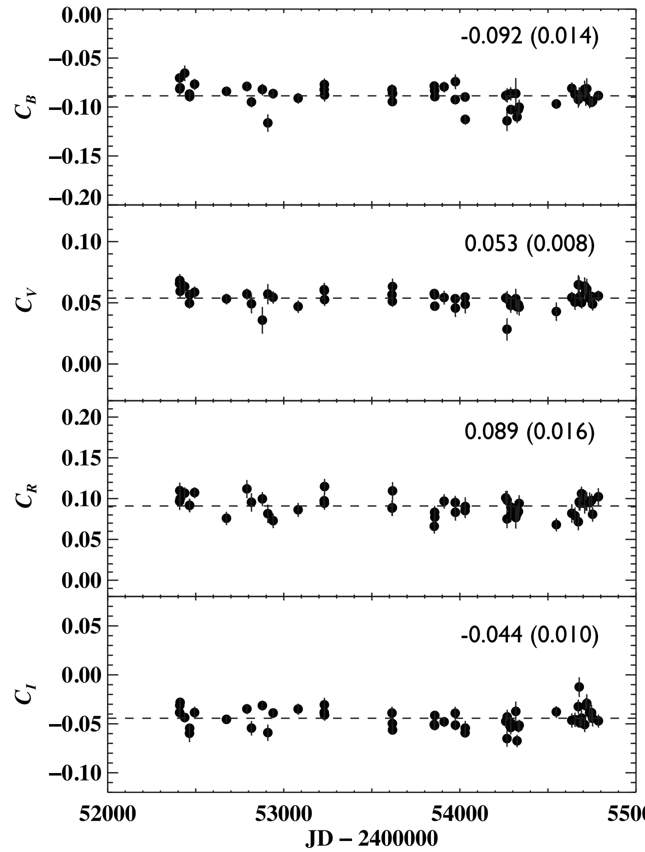

Figure 5. Same as Figure 4 except for the Nickel telescope.

Table 5
Wavelength Shifts to Instrumental Response Curves

Telescope/Filter Set	*B*	*V*	*R*	*I*
KAIT1 (Apogee/Old *BVRI*)	47 red	4 red	2 red	140 red
KAIT2 (Apogee/New *BVRI*)	35 red	12 red	2 red	0
KAIT3 (Apogee2/New *BVRI*)	15 blue	3 red	13 blue	21 blue
KAIT4 (FLI/New *BVRI*)	8 red	19 blue	41 blue	59 blue
1 m Nickel	66 red	46 red	38 red	80 red

Note. All shifts measured in Angstroms.

Discerning any trend in the evolution of the KAIT color terms is more difficult. Having four different CCD/filter combinations with varying tenures on KAIT, we do not have as long a baseline in comparison with the Nickel. We also do not have as many nights of photometric observations to determine the color terms. With the limited amount of available data, we do not detect any significant evolution in the color terms.

As a check on our color terms, we also derive the color terms needed to transform our natural-system magnitudes to the Landolt system using the total response curves for KAIT [1-4] and the Nickel. Armed with the atlas of spectrophotometric standards presented by Stritzinger et al. (2005), we calculate synthetic photometry for a number of standard stars over a range of colors using the transmission functions for KAIT[1-4] and the Nickel. The color terms derived from our synthetic photometry can be found in Table 4 along with the observed color terms derived from observations of Landolt standards on photometric nights.

Overall, the color terms derived from spectrophotometry match those derived from our observations of Landolt standards. The largest difference is in C_B for the Nickel telescope. The transmission functions for the Nickel filters are taken from the Mt. Hamilton Lick Observatory Web site and are the least well known, which could explain the rather significant difference. The other smaller differences are most likely due to other optical elements in the light path, such as the mirror reflectivity, which are not included in our transmission curve. Following Stritzinger et al. (2002), we shifted the throughput curves in wavelength until we recovered the observed color terms. The required shifts can be found in Table 5. In general, relatively small shifts (<100 Å) were required to match the observed color terms. The only exception is the *I* band of KAIT1 which required a shift of 140 Å.

3.5.2. Evolution of the Atmospheric Term

For each photometric night, we derive the atmospheric correction term required to do absolute photometry for calibrating our fields. We plot this as a function of time in Figure 6. There is no clear evolution over time. As a function of season, however, we do see evidence for a weak sinusoidal trend. Curiously, the atmospheric term is larger in the summer and fall months compared to the winter and spring months, contrary to the expectation that summer brings clearer, more transparent nights; the presence of diffuse smoke from various wildfires in California is a possible cause. This trend is small and will not impact our final photometry. We also caution that the inhomogeneous sampling (we have more photometric nights during the spring and summer months) could lead to a spurious trend.

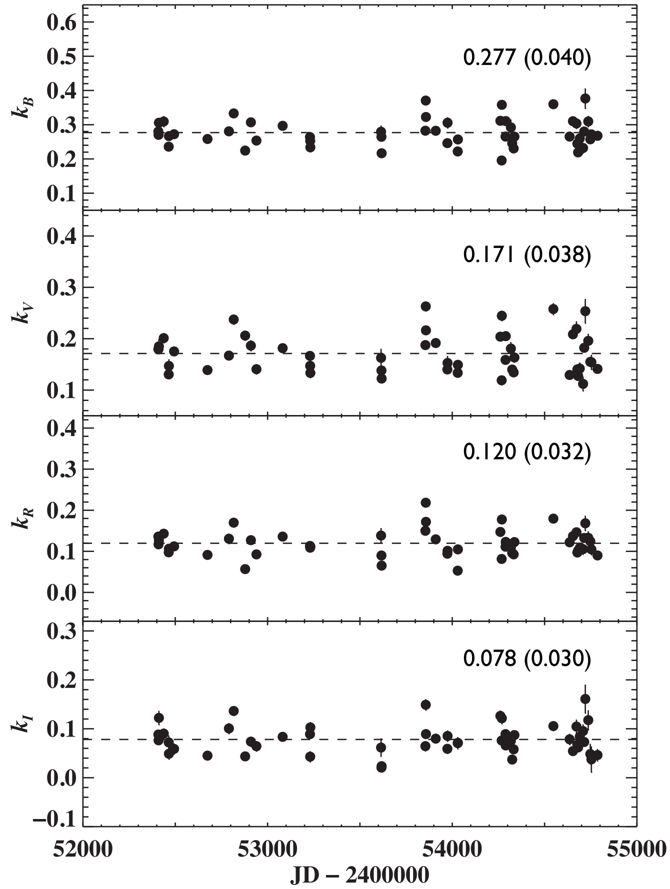

Figure 6. Atmospheric correction term for transforming Nickel natural-system magnitudes to the Landolt system as a function of time. We do not see a significant trend with time.

3.5.3. Combining Calibrations from KAIT and Nickel

Calibration of local standards in each SN field was done using both KAIT and the Nickel telescope. The results are combined using a sigma clipping routine to discard outliers. However, any systematic differences in photometry between different systems could translate into a systematic error in our final photometry depending on the ratio of the number of KAIT calibrations to Nickel calibrations. To quantify any differences in derived magnitudes for local standards between different systems, we compared the mean magnitude of each local standard using unique filter/CCD/telescope combinations. We only use instances in which a star was observed by two different systems. We find that there is no significant systematic shift between any of our different systems. We find a typical scatter of ∼0.03 mag in the distribution of mean magnitudes from different systems, which we adopt as our systematic uncertainty in all bands. Figure 7 shows the distribution in differences for local standard stars between Nickel and KAIT3, the two systems which share the most overlap in observed stars. The mean of the distribution for each filter is <0.01 mag with a $\sigma \approx 0.03$ mag. We find similar results in comparisons with our other systems.

3.5.4. Galaxy Subtraction

Even under the assumption that our galaxy subtraction routines are perfect, our ability to measure the SN magnitude is limited by the finite S/N of the template image. This induces a correlated error between photometry epochs that will affect parameters measured from light curves (e.g., Δm_{15}). To estimate this effect, we examined a test case where the SN occurred in an early-type galaxy having isophotes that could be easily measured. Using algorithms developed by Krajnović et al. (2006), we determined the isophote along the position of the SN.[6] Artificial stars with the same PSF as the SN were injected along the isophote in each data image, and the image was then reprocessed by our pipeline. We find that the scatter in the re-extraction of the artificial stars is comparable to the scatter we find in placing the artificial stars randomly within 60 pixels of the SN.

The previous method to gauge the error in the amount of galaxy light subtracted relies on the original measurement of the SN magnitude being correct. If the initial measurement is inaccurate, then the derived error from the scatter in our artificial-star test will not be indicative of the error induced from a galaxy template of the finite S/N. To further investigate the error in using only a single template, we reduced data for one SN with a deeper galaxy template having a higher S/N. The deeper template was made possible by searching through our photometry database for two SNe that exploded in the same galaxy spaced out by more than one year. KAIT followed both SN 2005ds and SN 2000cn which occurred in UGC 12177. We stacked 5–6 high-quality images (FWHM < 1″.5 with low sky background) of SN 2005ds to construct a deep galaxy template for UGC 12177, which we measure to be ∼1 mag deeper than a typical image from KAIT. We then ran the data for SN 2000cn through our pipeline using the deeper template with the same parameters adopted to reduce the data with a single image.

Figure 8 shows the results, with the top plot giving a comparison of the two final light curves. The middle plot shows the residual between the two light curves in *BVRI*, in the sense of the single-image template subtracted from the stacked template. The bottom plot is the residual scaled by the photometry error. Overall, the results from the two different galaxy templates are consistent with the error bars found using our pipeline. We do note, however, a few systematic trends. On average, there is a systematic difference of ∼0.04 mag in the *I* band, although this is almost always within 1σ. We also find that the *B*-band residuals increase with phase as the ratio of galaxy to SN flux increases at the position of the SN. However, the significance is reduced if we scale the residuals by the 1σ photometry error. We conclude from these tests that the correlated error induced from using a single image as a galaxy template is not negligible, but is taken into account by the error budget described in Section 3.4.

3.5.5. PSF as a Function of Color

We tested to see if there were variations of the PSF with the color of field stars. Using images of the open cluster M67, we measured the FWHM of stars taken from Chevalier & Ilovaisky (1991), which span a range of colors. A linear fit shows no convincing trend in either the KAIT or Nickel images. Figure 9 shows an example from data taken with the Nickel telescope. We rule out any strong dependence of the PSF on the color of field stars which would introduce a systematic error in our galaxy subtraction process.

3.5.6. Transformation into the Landolt System

A possible risk in transforming instrumental magnitudes into the Landolt system is correlating the SN magnitude with the color of the comparison local standard star. We check for

[6] An IDL version of the software is available from http://www-astro.physics.ox.ac.uk/~dxk/idl/.

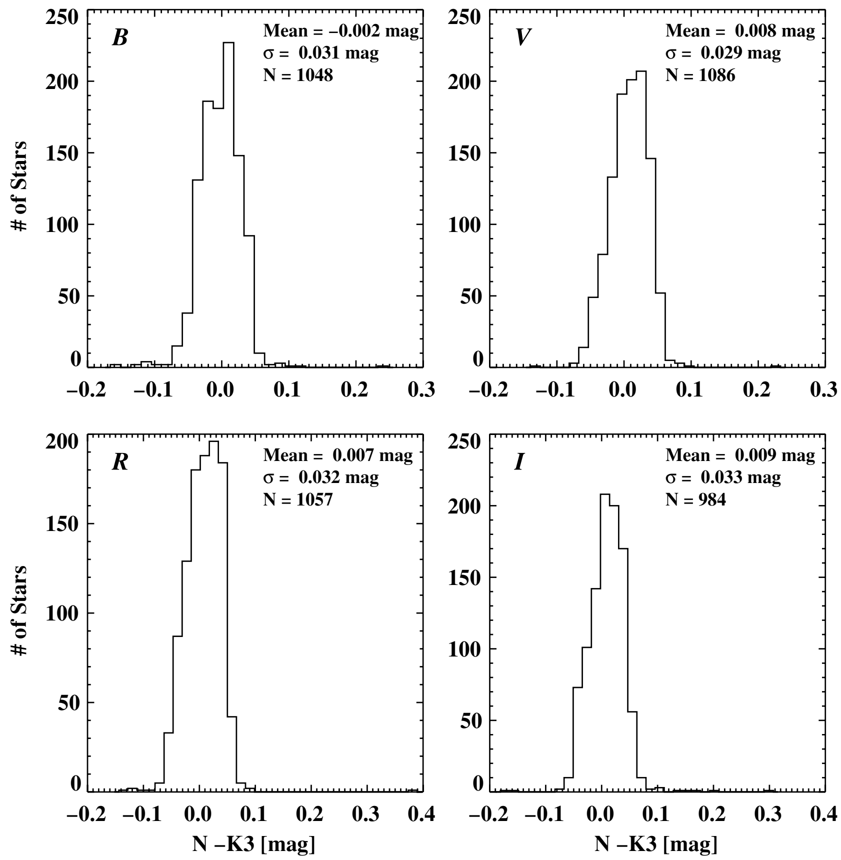

Figure 7. Distributions of residual differences in measurements of local standard stars observed with the Nickel telescope and KAIT3. The data are consistent with little to no offset in calibrations from these two different telescope systems in all observed bands. The scatter in the distributions leads us to adopt a systematic error of 0.03 mag.

any correlation in the post-transformation SN magnitude by calculating the χ^2 statistic defined as

$$\chi^2 = \sum_i \left(\frac{(m_i - \overline{m})}{\sigma_{m_i}} \right)^2,$$

where m_i is the SN magnitude found using the ith local standard star, $\overline{m}$ is the error-weighted average of SN magnitudes, and σ_{m_i} is the associated error in m_i (photometry and calibration error added in quadrature). We use the reduced χ^2, χ^2_ν, as an indicator to determine how well our final magnitudes are described by a constant (i.e., the error-weighted mean). We find that $\chi^2_\nu \approx 1$ in almost all cases, indicating that the error-weighted mean is an appropriate combination of individual measurements to produce a final SN magnitude. We do not see a convincing linear trend with the color of the comparison star; thus, we deem it unnecessary to correct our photometry for the possibility of this effect.

3.5.7. Summary

As a result of our study of possible systematic errors in our data set, we adopt a final systematic uncertainty of 0.03 mag in *BVRI*. This error is not included in our photometry tables, but should be included when combining the LOSS sample with photometry from other data sets.

4. RESULTS

We present the results of running the pipeline on SNe Ia from LOSS data taken during the interval 1998–2008. A representative sample of our light curves is shown in Figure 10. The light curves are shifted relative to the date of *B*-band maximum light found by using the light-curve fitting software MLCS2k2.v006 (Jha et al. 2007), or by direct polynomial fits for peculiar SNe that do not have representative templates in MLCS2k2.v006. An example of our photometry can be found in Table 6. We note that the uncertainty quoted in Table 6 only refers to the statistical error; a systematic error of 0.03 mag should be added when comparing to other data sets. Figure 11 shows an example of our finding charts, with comparison stars labeled. We include an example of our comparison-star photometry in Table 7. The complete versions of Figure 11 and Tables 6 and 7 are available in the online version of this article and are also available online.[7]

Basic information about each SN and galaxy was gathered from the NASA/IPAC Extragalactic Database (NED).[8] Discovery and classification information for each SN can be found in Table 8. Table 9 presents host-galaxy properties. Information regarding our SNe (such as discoverers, classification references, etc.) was obtained from our private searchable MYSQL SN database (J. M. Silverman et al. 2010, in preparation), which collects information about each SN.

4.1. The LOSS Sample

Precise measurements of cosmological parameters require multi-color light curves that are well sampled and range from

7 http://hercules.berkeley.edu/database/searchform_public.html
8 http://nedwww.ipac.caltech.edu/

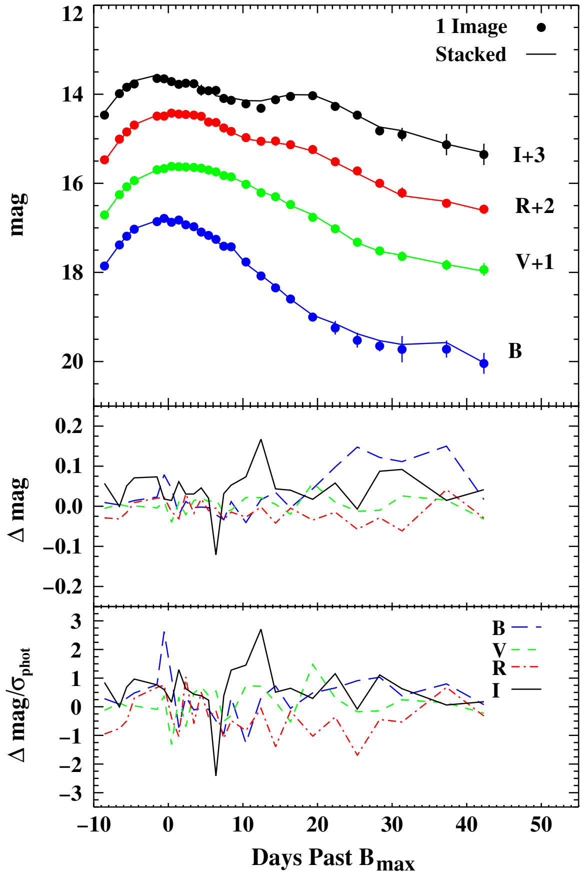

Figure 8. Comparison of reductions of SN 2000cn using a single template image and a stacked template of 5–6 images. The top plot is the two individual light curves. The middle portion shows the difference between the two reductions, in the sense of one template reduction minus the stacked template. The bottom plot shows the difference scaled by the photometry errors found from our pipelines.

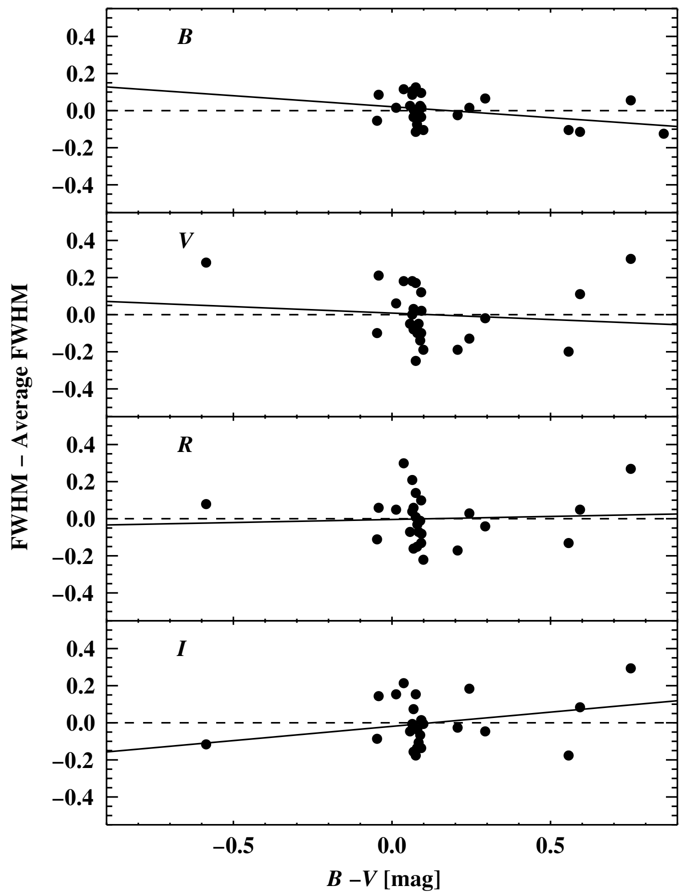

Figure 9. FWHM of stars in the field of M67 as a function of their color from *BVRI* images taken with the Nickel telescope. The best-fit line is plotted in solid black for each filter. We do not measure a significant trend, indicating that the image PSF is independent of color.

before maximum light to a month past maximum to accurately correlate the width of the light curve to its luminosity. Figure 12 shows the average cadence between photometry epochs versus the number of photometry epochs for each SN in our sample. The plot reveals a significant clustering around a cadence of 3 days and ∼25 epochs of photometry, indicating that our light curves are on average well sampled and cover an extensive range during the photometric evolution of the SN. A histogram of the number of photometry epochs can be found in Figure 13; we find a median of 21 epochs of photometry for the SNe. Figure 14 shows how many days after $B_{\max}$ we commence photometric monitoring. On average, we start observing 6 days before maximum light in B, with 125 SNe having data before maximum.

Cosmological studies of SNe Ia require follow-up observations of SNe that are within the Hubble flow to avoid substantial peculiar velocities induced by the gravitational attraction between galaxies, which produce deviations from a straight Hubble law. Adopting a typical peculiar velocity of 300 km s^{-1}, we define the lower limit of our cosmology sample at cz = 3000 km s^{-1}, at which point peculiar motions will be $\lesssim$10% of the expansion velocity. Our sample contains 135 SNe Ia in the Hubble flow. Figure 15 shows a histogram of the LOSS sample as a function of redshift. We find a median recession velocity of cz_{helio} = 5816 km s^{-1} for our entire sample, and a median value of cz_{helio} = 6595 km s^{-1} for our Hubble-flow sample.

4.2. Comparison with Published Data

In this paper, we present a homogeneously observed and reduced data set of SN Ia *BVRI* light curves. The most productive science will come from combining data sets collected from different telescopes (Kowalski et al. 2008; Hicken et al. 2009a). Understanding the underlying differences between these data sets will be crucial to improving the cosmological utility of SNe Ia. Wang et al. (2009b) have shown that photometry of a nearby bright SN ($B_{\max}$ = 13.64 mag) having negligible host-galaxy contamination with different telescopes can exhibit systematic differences of $\sigma \approx$ 0.05 mag prior to making S-corrections for instrumental response (Stritzinger et al. 2002). The situation becomes increasingly more complicated when galaxy subtraction must be performed.

While it is outside the scope of this paper to conduct a detailed comparison to quantify systematic differences between reductions of common SNe, it is instructive to do a rough comparison to what has been published in the literature as a sanity check on our pipeline reductions. We classify the level or concordance by the following definitions: “good” is an average difference within 0.05 mag, “adequate” is between 0.05 mag and 0.1 mag, and “poor” is greater than 0.1 mag. In the following comparison, we include the systematic error of 0.03 mag found in Section 3.5.

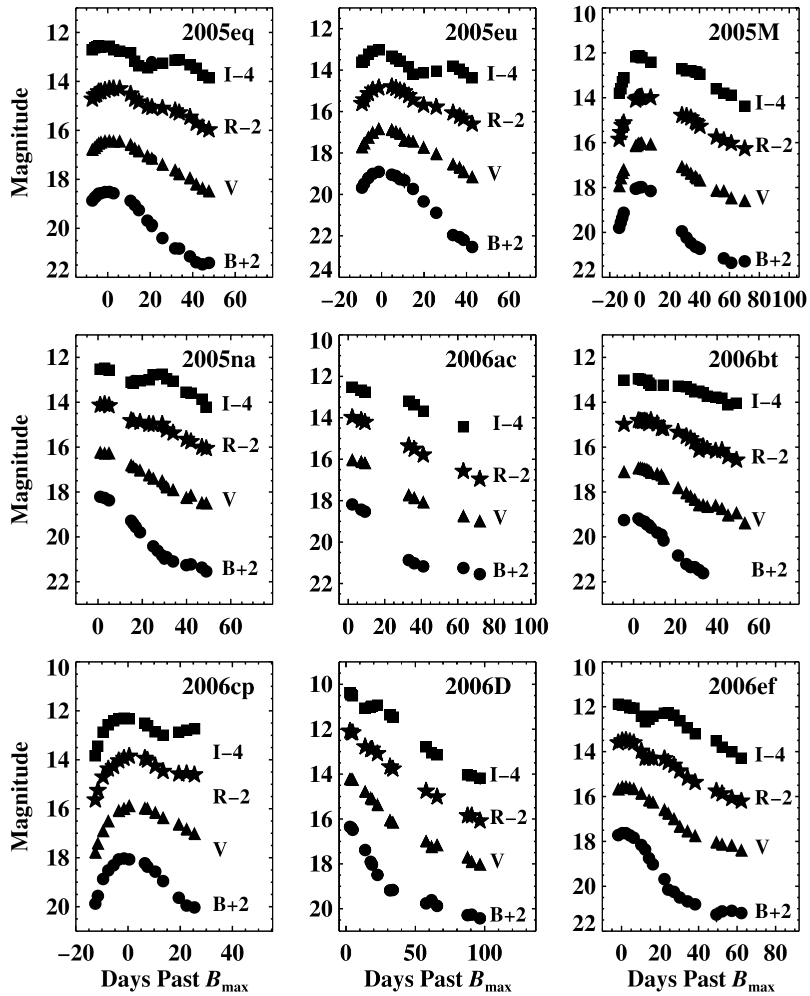

Figure 10. Representative *BVRI* light curves of nine SNe Ia from our sample. Dates have been shifted relative to B_{max}.

4.2.1. Comparisons to Previous LOSS Reductions

A few of the SNe included herein have been reduced manually by other members of our research group. Comparing the results from our pipeline to previously published KAIT and Nickel data offers a unique check on our pipeline without having to worry about the difficulties that arise from comparing photometry from different telescopes.

Optical light curves of SN 1998de using KAIT data were published by Modjaz et al. (2001). SN 1998de was a subluminous SN 1991bg-like object (Filippenko et al. 1992a; Leibundgut et al. 1993) located 72″ from the nucleus of its host galaxy ($cz = 4990$ km s^{-1}) in a clean environment free of galaxy contamination. Neither reduction procedure used template subtraction and both utilized PSF-fitting photometry. Our comparison-star calibrations agree to within 0.01 mag in *BVR*, although our *I*-band calibration is systematically 0.03 mag brighter. The photometry published by Modjaz et al. is *K*-corrected and cannot be compared directly to the data presented here. We obtained the original (not *K*-corrected) data directly from the lead author, M. Modjaz (2010, private communication). Our results agree to within 0.01 mag in *BVR*. Our *I*-band photometry is brighter by ∼0.05 mag, which is not entirely unexpected since our field calibration is systemically brighter in *I* by 0.03 mag.

KAIT light curves for the peculiar SN 2000cx were published by Li et al. (2001c). A bright, nearby (but peculiar) SN Ia located far from the nucleus of its host galaxy, both reductions did not perform galaxy subtraction and used PSF-fitting photometry. The *BVRI* light curves agree to within 0.03 mag. It is also worth noting that the pipeline reduction brings the KAIT data to within 0.01 mag of *BVRI* data obtained at the Wise Observatory (Israel) that were also presented by Li et al.

SN 2002bf provides an excellent test of the abilities of our pipeline. The SN lies 4″.1 from its host galaxy's center. Leonard et al. (2005) present photometry from KAIT and the Nickel telescope which were rereduced with our photometry pipeline. As is noted by the authors of Leonard et al., "the galaxy subtraction procedure for SN 2002bf was particularly challenging." In Figure 16, we compare our reduction to that of Leonard et al. In general, we find a systematic offset of ∼0.1 mag in all bands; it is most pronounced in the late-time data when proper galaxy subtraction is the most necessary. The final magnitudes for both sets of comparison stars show excellent agreement. The discrepancy can probably be traced back to the galaxy subtraction. Examining the results of our pipeline, we do not see any obvious results of oversubtraction which could explain why we systematically measure the SN to be fainter than found by Leonard et al.

Leonard et al. (2005) present *BVRI* light curves of SN 2003du taken by KAIT and the Nickel telescope, but reduced manually without the use of the pipeline. The two reductions are in excellent agreement, to within 0.01 mag in *BVR* and within

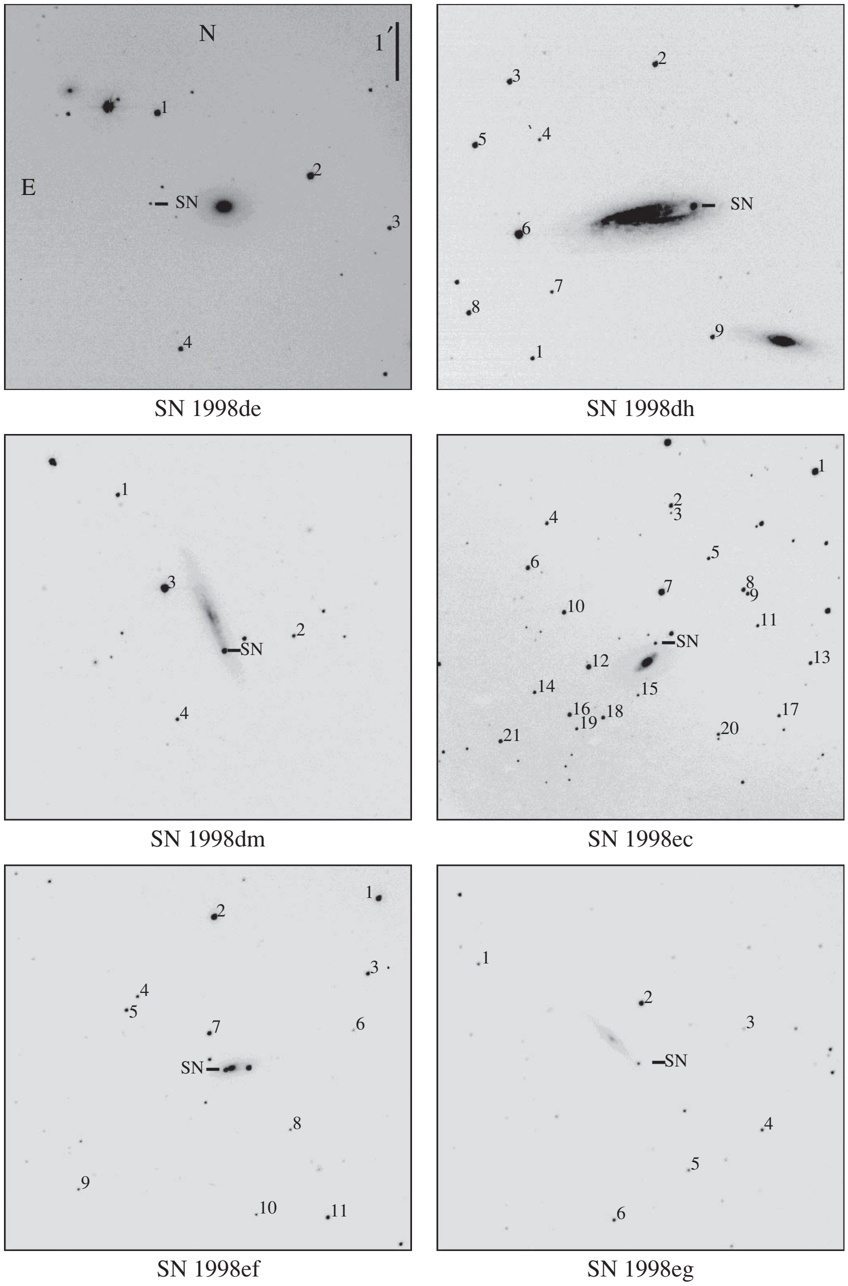

Figure 11. Finder charts for six SNe Ia from our sample. The vertical bar on the right edge of the top-left panel indicates 1′. North is up and east to the left. Finders for the rest of our sample are archived with the journal.

(An extended version of this figure is available in the online journal.)

0.03 mag in *I*. Our *I*-band data are systematically brighter than those published by Leonard et al. Although this is within our definition of "good," the difference in *I* is troubling. The solution is likely traced back to the calibrations of the local standards. While there is general agreement between the new and old calibrations in *I*, our star 7 is brighter than star 6 of Leonard et al. by 0.1 mag, and our star 9 is brighter by 0.03 mag, which would make our *I*-band photometry of SN 2003du brighter. This exercise highlights the importance of calibrations in producing reliable SN flux measurements.

SN 2005cf data taken with KAIT were reduced independently by Wang et al. (2009b). The SN is sufficiently far away from the host-galaxy nucleus that galaxy subtraction was not performed by either reduction. The two reductions are in excellent agreement, with *BVRI* photometry all within 0.01 mag.

4.2.2. Comparison to CfA2

Jha et al. (2006b) present *UBVRI* light curves of 44 SNe Ia from the CfA2 data set, of which 17 can be found in the LOSS sample. Of the 17, 15 have overlapping data which can be compared. We compare the two data sets by interpolating a line between LOSS data taken within at most 4 days from each CfA2 data point. We include a systematic error of 0.02 mag for the CfA2 data based on they systematic error found for CfA3 data (Hicken et al. 2009b).

Overall, we find good agreement between the two data sets with a few exceptions. In particular, SNe 1998dh, 1999aa,

Table 6
Photometry of SN 2001dl

JD	B (mag)	V (mag)	R (mag)	I (mag)	Telescope
2452121.83	17.942 (083)	17.665 (052)	17.265 (029)	16.985 (039)	KAIT2
2452122.81	17.658 (040)	17.381 (051)	17.035 (028)	16.862 (031)	KAIT2
2452123.80	17.512 (037)	17.255 (029)	16.828 (019)	16.650 (031)	KAIT2
2452124.79	17.350 (062)	17.082 (033)	16.749 (028)	16.574 (035)	KAIT2
2452128.88	17.089 (038)	16.766 (021)	16.517 (020)	16.391 (032)	KAIT2
2452129.84	17.137 (049)	16.758 (028)	16.463 (021)	16.484 (040)	KAIT2
2452130.86	17.022 (034)	16.766 (024)	16.462 (016)	16.513 (025)	KAIT2
2452132.81	17.076 (025)	16.760 (025)	16.450 (015)	16.604 (066)	KAIT2
2452134.74	17.138 (031)	16.765 (018)	16.496 (013)	16.708 (038)	KAIT2
2452136.82	17.292 (027)	16.827 (017)	16.587 (022)	16.825 (049)	KAIT2
2452138.78	17.297 (030)	16.884 (022)	16.656 (013)	16.952 (038)	KAIT2
2452140.81	17.478 (048)	17.022 (020)	16.820 (015)	17.030 (043)	KAIT2
2452142.77	17.617 (026)	17.100 (029)	16.985 (031)	17.280 (081)	KAIT2
2452145.82	17.992 (086)	17.334 (042)	17.170 (023)	17.333 (061)	KAIT2
2452147.76	18.095 (064)	17.393 (025)	17.236 (034)	17.495 (078)	KAIT2
2452151.72	18.574 (092)	17.576 (043)	17.313 (040)	17.328 (065)	KAIT2
2452157.79	19.177 (129)	17.884 (065)	17.360 (030)	17.088 (044)	KAIT2
2452161.74	19.527 (124)	18.159 (056)	17.559 (029)	17.079 (049)	KAIT2
2452165.76	19.836 (058)	18.366 (035)	17.704 (030)	17.220 (034)	KAIT3
2452169.72	19.878 (097)	18.637 (052)	17.983 (030)	17.482 (038)	KAIT3
2452173.68	20.027 (123)	18.766 (067)	18.173 (035)	17.758 (040)	KAIT3
2452182.70	...	...	18.526 (131)	...	KAIT3
2452186.67	...	18.875 (081)	18.575 (044)	18.412 (082)	KAIT3

Note. Quoted errors in parentheses are in units of 0.001 mag.

(This table is available in its entirety in a machine-readable form in the online journal. A portion is shown here for guidance regarding its form and content.)

Table 7
Comparison Stars

Star	α(J2000)	δ(J2000)	B (mag)	V (mag)	R (mag)	I (mag)	N_{calib}
			SN 2002de				
SN	$16^{\mathrm{h}}16^{\mathrm{m}}30\overset{\mathrm{s}}{.}38$	$+35°42'30\overset{''}{.}2$					
1	16:16:33.47	+35:40:34.1	18.221(011)	16.775(014)	15.878(012)	15.038(010)	5
2	16:16:20.58	+35:45:32.8	16.595(011)	15.794(013)	15.379(013)	15.001(009)	4
3	16:16:38.51	+35:45:21.5	17.980(010)	17.454(014)	17.066(011)	16.781(014)	4
4	16:16:23.30	+35:45:16.9	17.442(013)	16.897(012)	16.556(011)	16.255(013)	5
5	16:16:18.33	+35:44:26.6	17.346(012)	16.710(011)	16.363(010)	16.053(013)	5
6	16:16:45.44	+35:43:20.6	16.332(007)	15.632(013)	15.244(010)	14.859(011)	4
7	16:16:30.30	+35:41:24.6	17.384(011)	16.770(013)	16.376(009)	16.099(016)	6

Note. Quoted errors in parentheses are in units of 0.001 mag.

(This table is available in its entirety in a machine-readable form in the online journal. A portion is shown here for guidance regarding its form and content.)

2000cn, 1999ac, 1999dq, 1999ej, 1999gp, and 2000cn all agree to within 0.05 mag.

The worst cases of systematic differences are found in the I band. We find differences of ~0.1 mag for SNe 1998ef, 1998es, 1999cl, 1999gh, 2000dk, and 2000fa. With the exception of SN 1999cl, the LOSS data are systematically fainter than the CfA2 data. Comparing our derived magnitudes for the field stars to those of Jha et al., we find no discernible trend to explain the magnitude of the discrepancy.

In the case of SN 1999cl, the likely culprit is the calibration. We have only three comparison stars in our calibration (typically we have ~10 stars in a field), of which two overlap with the CfA2. Our star 2 is fainter than their star 4 by 0.07 mag. A summary of our comparison to Jha et al. can be found in Table 10.

The most likely solution is to apply S-corrections (Stritzinger et al. 2002) in order to account for the variation in transmission functions of different telescopes. Wang et al. (2009b) show that the scatter in the I-band light curve of SN 2005cf, combining data from seven different telescopes, is reduced from 0.061 mag to 0.030 mag by applying S-corrections. If S-corrections are indeed the explanation of the differences between the LOSS and CfA2 data, we would expect the residual to be dependent on the spectral energy distribution of the SN. In Figures 17–19, we compare the BRI residuals to $B - V$, $V - R$, and $V - I$ colors (respectively) for all of the data points in our overlapping set of SNe. In Figures 17 and 18, the B and R residuals are fairly independent of color. Subtracting the linear fit to the data points to remove any perceived linear correlation does not improve the scatter. However, doing so for the I-band residuals reduces the scatter from 0.084 to 0.075 mag, hinting that applying a color-dependent S-correction might slightly improve the situation.

4.2.3. SN 2002bo

Krisciunas et al. (2004) present optical photometry of SN 2002bo. We find that our photometry is in good agreement;

Table 8
Discovery and Classification References for SNe Ia in the LOSS Sample

SN	Host Galaxy	UT Discovery Date	Discovery Ref.	Spectroscopic Ref.
SN 1998de	NGC 252	1998 Jul 23	IAUC 6977	IAUC 6980
SN 1998dh	NGC 7541	1998 Jul 20	IAUC 6978	IAUC 6980
SN 1998dm	MCG -01-4-44	1998 Aug 22	IAUC 6993	IAUC 6997
SN 1998ec	UGC 3576	1998 Sep 26	IAUC 7022	IAUC 7024
SN 1998ef	UGC 646	1998 Oct 18	IAUC 7032	IAUC 7032
SN 1998eg	UGC 12133	1998 Oct 19	IAUC 7033	IAUC 7037
SN 1998es	NGC 632	1998 Nov 13	IAUC 7050	IAUC 7054
SN 1999aa	NGC 2595	1999 Feb 11	IAUC 7108	IAUC 7108
SN 1999ac	NGC 6063	1999 Feb 26	IAUC 7114	IAUC 7122
SN 1999bh	NGC 3435	1999 Mar 29	IAUC 7135	IAUC 7138
SN 1999by	NGC 2841	1999 Apr 30	IAUC 7156	IAUC 7157
SN 1999cl	NGC 4501	1999 May 29	IAUC 7185	IAUC 7190
SN 1999cp	NGC 5468	1999 Jun 18	IAUC 7205	IAUC 7206
SN 1999da	NGC 6411	1999 Jul 5	IAUC 7215	IAUC 7219
SN 1999dg	UGC 9758	1999 Jul 23	IAUC 7229	IAUC 7239
SN 1999dk	UGC 1087	1999 Aug 12	IAUC 7237	IAUC 7238
SN 1999dq	NGC 976	1999 Sep 2	IAUC 7247	IAUC 7250
SN 1999ej	NGC 495	1999 Oct 18	IAUC 7286	IAUC 7298
SN 1999gh	NGC 2986	1999 Dec 3	IAUC 7286	IAUC 7328
SN 1999gp	UGC 1993	1999 Dec 23	IAUC 7337	IAUC 7341
SN 2000cn	UGC 11064	2000 Jun 2	IAUC 7436	IAUC 7437
SN 2000cp	2MFGC 12921	2000 Jun 21	IAUC 7441	IAUC 7442
SN 2000cu	ESO 525-G004	2000 Jul 12	IAUC 7453	IAUC 7454
SN 2000cw	MCG +05-56-7	2000 Jul 14	IAUC 7456	IAUC 7457
SN 2000cx	NGC 524	2000 Jul 17	IAUC 7458	IAUC 7463
SN 2000dg	MCG +01-1-29	2000 Aug 22	IAUC 7480	IAUC 7484
SN 2000dk	NGC 382	2000 Sep 18	IAUC 7493	IAUC 7494
SN 2000dm	UGC 11198	2000 Sep 24	IAUC 7495	IAUC 7497
SN 2000dn	IC 1468	2000 Sep 27	IAUC 7498	IAUC 7499
SN 2000dr	IC 1610	2000 Oct 5	IAUC 7505	IAUC 7506
SN 2000fa	UGC 3770	2000 Nov 30	IAUC 7533	IAUC 7535
SN 2001C	CGCG 285-012	2001 Jan 4	IAUC 7555	IAUC 7563
SN 2001E	NGC 3905	2001 Jan 5	IAUC 7557	IAUC 7566
SN 2001V	NGC 3987	2001 Feb 19	IAUC 7585	IAUC 7585
SN 2001ah	UGC 6211	2001 Mar 27	IAUC 7603	IAUC 7604
SN 2001ay	IC 4423	2001 Apr 18	IAUC 7611	IAUC 7612
SN 2001bf	MCG +04-42-22	2001 May 3	IAUC 7620	IAUC 7625
SN 2001bg	NGC 2608	2001 May 8	IAUC 7621	IAUC 7622
SN 2001bp	SDSS J160208.91+364313.8	2001 May 15	IAUC 7626	IAUC 7626
SN 2001br	UGC 11260	2001 May 13	IAUC 7629	IAUC 7629
SN 2001cj	UGC 8399	2001 May 30	IAUC 7640	IAUC 7651
SN 2001ck	UGC 9425	2001 Jun 3	IAUC 7641	IAUC 7645
SN 2001cp	UGC 10738	2001 Jun 19	IAUC 7645	IAUC 7640
SN 2001da	NGC 7780	2001 Jul 9	IAUC 7658	IAUC 7664
SN 2001dl	UGC 11725	2001 Jul 30	IAUC 7675	IAUC 7676
SN 2001eh	UGC 1162	2001 Sep 9	IAUC 7714	IAUC 7714
SN 2001en	NGC 523	2001 Sep 26	IAUC 7724	IAUC 7732
SN 2001ep	NGC 1699	2001 Oct 3	IAUC 7727	IAUC 7731
SN 2001ex	UGC 3595	2001 Oct 16	IAUC 7735	IAUC 7736
SN 2001fh	2MASX J21204248+4423590	2001 Nov 3	IAUC 7744	IAUC 7748
SN 2002G	CGCG 189-024	2002 Jan 18	IAUC 7797	IAUC 7802
SN 2002aw	2MFGC 13321	2002 Feb 15	IAUC 7831	IAUC 7834
SN 2002bf	CGCG 266-031	2002 Feb 22	IAUC 7836	IAUC 7846
SN 2002bo	NGC 3190	2002 Mar 9	IAUC 7847	IAUC 7848
SN 2002cd	NGC 6916	2002 Apr 8	IAUC 7871	IAUC 7873
SN 2002cf	NGC 4786	2002 Apr 13	IAUC 7877	IAUC 7878
SN 2002cr	NGC 5468	2002 May 1	IAUC 7890	IAUC 7891
SN 2002cs	NGC 6702	2002 May 5	IAUC 7891	IAUC 7894
SN 2002cu	NGC 6575	2002 May 11	IAUC 7898	IAUC 7898
SN 2002cx	CGCG 044-035	2002 May 12	IAUC 7902	IAUC 7903
SN 2002de	NGC 6104	2002 Jun 1	IAUC 7914	IAUC 7915
SN 2002dj	NGC 5018	2002 Jun 12	IAUC 7918	IAUC 7919
SN 2002dl	UGC 11994	2002 Jun 16	IAUC 7920	IAUC 7923
SN 2002do	MCG +07-41-1	2002 Jun 17	IAUC 7923	IAUC 7927
SN 2002dp	NGC 7678	2002 Jun 18	IAUC 7924	IAUC 7927
SN 2002eb	CGCG 473-011	2002 Jul 22	IAUC 7937	IAUC 7953

Table 8
(Continued)

SN	Host Galaxy	UT Discovery Date	Discovery Ref.	Spectroscopic Ref.
SN 2002ef	NGC 7761	2002 Jul 30	IAUC 7943	IAUC 7945
SN 2002el	NGC 6986	2002 Aug 12	IAUC 7953	IAUC 7954
SN 2002er	UGC 10743	2002 Aug 23	IAUC 7959	IAUC 7961
SN 2002eu	2MASXI J0149427+323730	2002 Aug 30	IAUC 7963	IAUC 7965
SN 2002fb	NGC 759	2002 Sep 6	IAUC 7967	IAUC 7967
SN 2002fk	NGC 1309	2002 Sep 17	IAUC 7973	IAUC 7976
SN 2002ha	NGC 6962	2002 Oct 21	IAUC 7997	IAUC 7999
SN 2002he	UGC 4322	2002 Oct 28	IAUC 8002	IAUC 8004
SN 2002jg	NGC 7253	2002 Nov 23	IAUC 8022	IAUC 8023
SN 2003D	MCG -01-25-9	2003 Jan 6	IAUC 8043	IAUC 8043
SN 2003W	UGC 5234	2003 Jan 28	IAUC 8061	IAUC 8061
SN 2003Y	IC 522	2003 Jan 29	IAUC 8062	IAUC 8063
SN 2003cg	NGC 3169	2003 Mar 21	IAUC 8097	IAUC 8099
SN 2003cq	NGC 3978	2003 Mar 30	IAUC 8103	IAUC 8106
SN 2003du	UGC 9391	2003 Apr 22	IAUC 8121	IAUC 8122
SN 2003fa	ARK 527	2003 Jun 1	IAUC 8140	IAUC 8142
SN 2003gn	CGCG 452-024	2003 Jul 22	IAUC 8168	IAUC 8170
SN 2003gq	NGC 7407	2003 Jul 24	IAUS 8168	IAUC 8170
SN 2003gs	NGC 936	2003 Jul 29	IAUC 8171	IAUC 8172
SN 2003gt	NGC 6930	2003 Jul 29	IAUC 8172	IAUC 8175
SN 2003he	MCG -01-1-10	2003 Aug 11	IAUC 8182	IAUC 8189
SN 2003hv	NGC 1201	2003 Sep 9	IAUC 8197	IAUC 8198
SN 2003kf	MCG -02-16-2	2003 Nov 27	CBET 53	CBET 53
SN 2004E	KUG 1314+318B	2004 Jan 15	IAUC 8271	IAUC 8271
SN 2004S	MCG -05-16-21	2004 Feb 3	IAUC 8283	IAUC 8283
SN 2004as	SDSS J112538.81+224952.2	2004 Mar 11	IAUC 8302	IAUC 8302
SN 2004at	MCG +10-16-37	2004 Mar 12	IAUC 8302	IAUC 8304
SN 2004bd	NGC 3786	2004 Apr 7	IAUC 8316	IAUC 8317
SN 2004bg	UGC 6363	2004 Apr 7	IAUC 8317	IAUC 8321
SN 2004bk	NGC 5246	2004 Apr 22	IAUC 8329	IAUC 8331
SN 2004br	NGC 4493	2004 May 15	IAUC 8340	IAUC 8343
SN 2004bv	NGC 6907	2004 May 24	IAUC 8344	IAUC 8345
SN 2004bw	MCG +00-38-19	2004 May 26	IAUC 8345	IAUC 8353
SN 2004dt	NGC 799	2004 Aug 11	IAUC 8386	IAUC 8387
SN 2004ef	UGC 12158	2004 Sep 4	IAUC 8399	IAUC 8403
SN 2004eo	NGC 6928	2004 Sep 17	IAUC 8406	IAUC 8409
SN 2004ey	UGC 11816	2004 Oct 14	IAUC 8419	IAUC 8420
SN 2004fz	NGC 783	2004 Nov 14	IAUC 8437	IAUC 8440
SN 2004gs	MCG +03-22-20	2004 Dec 12	IAUC 8453	IAUC 8453
SN 2005M	NGC 2930	2005 Jan 19	IAUC 8470	IAUC 8474
SN 2005am	NGC 2811	2005 Feb 22	IAUC 8490	IAUC 8491
SN 2005bc	NGC 5698	2005 Apr 2	IAUC 8504	CBET 132
SN 2005bl	NGC 4070	2005 Apr 14	IAUC 8512	CBET 139
SN 2005bo	NGC 4708	2005 Apr 17	IAUC 8514	IAUC 8517
SN 2005cc	NGC 5383	2005 May 19	IAUC 8534	ATEL 502
SN 2005cf	MCG -01-39-3	2005 May 28	IAUC 8534	IAUC 8534
SN 2005de	UGC 11097	2005 Aug 2	IAUC 8580	IAUC 8581
SN 2005dm	IC 219	2005 Aug 26	IAUC 8589	CBET 204
SN 2005el	NGC 1819	2005 Sep 25	IAUC 8604	CBET 245
SN 2005eq	MCG -01-9-6	2005 Sep 30	IAUC 8608	IAUC 8610
SN 2005eu	NSF J022743.32+281037.6	2005 Oct 4	IAUC 8611	CBET 245
SN 2005na	UGC 3634	2005 Dec 31	IAUC 8655	CBET 351
SN 2006D	MCG -01-33-34	2006 Jan 11	CBET 362	CBET 366
SN 2006X	NGC 4321	2006 Feb 4	IAUC 8667	CBET 393
SN 2006ac	NGC 4619	2006 Feb 9	IAUC 8669	CBET 398
SN 2006bt	CGCG 108-013	2006 Apr 26	CBET 485	CBET 485
SN 2006cp	UGC 7357	2006 May 28	CBET 524	CBET 528
SN 2006dm	MCG -01-60-21	2006 Jul 3	CBET 568	CBET 569
SN 2006ef	NGC 809	2006 Aug 18	CBET 597	CBET 604
SN 2006ej	NGC 191	2006 Aug 23	CBET 603	CBET 604
SN 2006em	NGC 911	2006 Aug 25	CBET 605	CBET 612
SN 2006en	MCG +05-54-41	2006 Aug 26	CBET 606	CBET 608
SN 2006eu	MCG +08-36-16	2006 Sep 3	IAUC 8745	CBET 622
SN 2006gr	UGC 12071	2006 Aug 21	CBET 638	CBET 642
SN 2006hb	MCG -04-12-34	2006 Sep 27	CBET 649	CBET 652
SN 2006je	IC 1735	2006 Oct 15	CBET 675	CBET 678

Table 8
(Continued)

SN	Host Galaxy	UT Discovery Date	Discovery Ref.	Spectroscopic Ref.
SN 2006le	UGC 3218	2006 Oct 26	CBET 700	CBET 702
SN 2006lf	UGC 3108	2006 Oct 26	CBET 704	CBET 705
SN 2007O	UGC 9612	2007 Jan 21	CBET 818	CBET 818
SN 2007af	NGC 5584	2007 Mar 1	CBET 863	CBET 865
SN 2007au	UGC 3725	2007 Mar 18	CBET 895	CBET 898
SN 2007bc	UGC 6332	2007 Apr 4	CBET 913	CBET 915
SN 2007bj	NGC 6172	2007 Apr 18	CBET 930	IAUC 8834
SN 2007ca	MCG -02-34-61	2007 Apr 25	CBET 945	CBET 947
SN 2007ci	NGC 3873	2007 May 15	CBET 966	IAUC 8843
SN 2007co	MCG +05-43-16	2007 Jun 4	CBET 977	CBET 978
SN 2007cq	2MASX J22144070+0504435	2007 Jun 21	CBET 983	CBET 984
SN 2007fr	UGC 11780	2007 Jul 14	CBET 1001	CBET 1001
SN 2007hj	NGC 7461	2007 Sep 1	CBET 1048	CBET 1048
SN 2007le	NGC 7721	2007 Oct 13	CBET 1100	CBET 1101
SN 2007sr	NGC 4038	2007 Dec 18	CBET 1172	CBET 1173
SN 2007qe	NSF J235412.09+272432.3	2007 Nov 13	CBET 1138	ATEL 1280
SN 2007ux	2MASX J10091969+1459268	2007 Dec 23	CBET 1187	CBET 1189
SNF20071021-000[a]	2MASX J00150006+1619596	2007 Oct 21	...	...
SN 2008A	NGC 634	2008 Jan 2	CBET 1193	CBET 1198
SN 2008C	UGC 3611	2008 Jan 3	CBET 1195	CBET 1197
SN 2008L	NGC 1259	2008 Jan 14	CBET 1212	CBET 1219
SN 2008Q	NGC 524	2008 Jan 26	CBET 1228	CBET 1232
SN 2008Z	SDSS J094315.36+361709.2	2008 Feb 7	CBET 1243	CBET 1246
SN 2008af	UGC 09640	2008 Feb 9	CBET 1248	CBET 1253
SN 2008ar	IC 3284	2008 Feb 27	CBET 1273	CBET 1273
SN 2008bf	NGC 4055	2008 Mar 18	CBET 1307	CBET 1310
SN 2008cl	UGC 10261	2008 May 16	CBET 1378	CBET 1380
SN 2008dr	NGC 7222	2008 Jun 28	CBET 1419	CBET 1419
SN 2008dt	NGC 6261	2008 Jun 30	CBET 1423	CBET 1424
SN 2008dx	NGC 4898A	2008 Jun 24	CBET 1427	CBET 1427
SN 2008ec	NGC 7469	2008 Jul 14	CBET 1437	CBET 1438
SN 2008ei	UGC 11977	2008 Jul 23	CBET 1446	CBET 1447
SNF20080514-002[a]	UGC 8472	2008 May 16	ATEL 1532	ATEL 1532
SNF20080909-030[a]	...	2008 Sep 9	...	...

Note. [a] Discovered and spectroscopically classified by the Nearby Supernova Factory (Aldering et al. 2002).

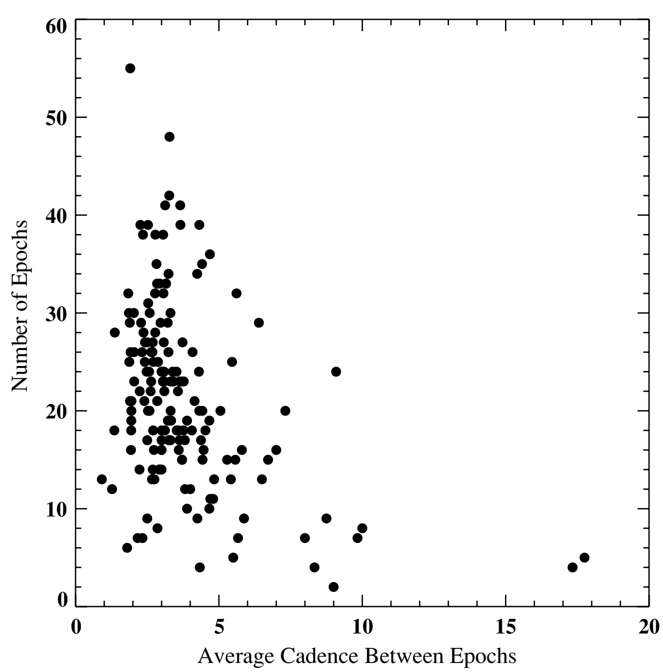

Figure 12. Scatterplot of the average cadence between epochs in days vs. the number of epochs for each SN. The tight grouping of points indicates that a large majority of the SNe are well sampled and have over 20 epochs of photometry.

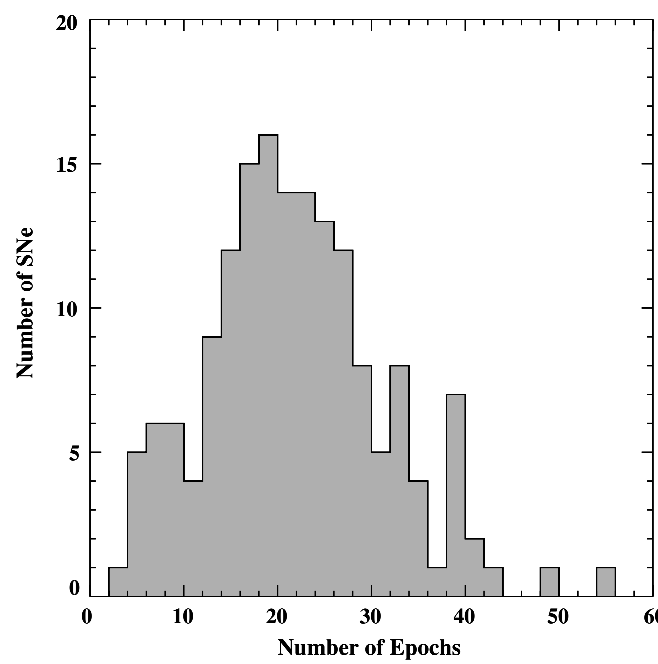

Figure 13. Distribution for the number of epochs per SN using the number of V-band observations. We find a median of 21 epochs of photometry per SN.

Table 9
Host-galaxy References for SNe Ia in the LOSS Sample

SN	Host	$E(B-V)_{\rm MW}$ (mag)	$z_{\rm helio}$	E (″)	N (″)
SN 1998de	S0	0.059	0.016	72	3
SN 1998dh	Sbc	0.067	0.009	−54	10
SN 1998dm	Sc	0.045	0.007	−14	−37
SN 1998ec	Sb	0.085	0.020	−9	20
SN 1998ef	Sb	0.074	0.018	6	−2
SN 1998eg	Sc	0.121	0.025	−26	−25
SN 1998es	S0	0.032	0.011	0	11
SN 1999aa	Sc	0.040	0.014	2	31
SN 1999ac	Scd	0.046	0.009	24	−30
SN 1999bh	Sb	0.015	0.017	−10	−3
SN 1999by	Sb	0.016	0.002	−98	89
SN 1999cl	Sb	0.038	0.008	−46	23
SN 1999cp	Scd	0.025	0.009	−52	23
SN 1999da	E	0.051	0.013	−71	1
SN 1999dg	S0	0.039	0.022	5	5
SN 1999dk	Sc	0.050	0.015	4	26
SN 1999dq	Sc	0.109	0.014	−4	−6
SN 1999ej	S0a	0.072	0.014	18	−20
SN 1999gh	E	0.058	0.008	52	16
SN 1999gp	Sb	0.056	0.027	−11	10
SN 2000cn	Scd	0.057	0.023	−7	−7
SN 2000cp	Sb	0.050	0.034	−3	2
SN 2000cu	Sa	0.088	0.020	12	2
SN 2000cw	Sbc	0.072	0.030	8	−21
SN 2000cx	S0	0.082	0.008	−23	−109
SN 2000dg	Sb	0.092	0.038	−7	−1
SN 2000dk	E	0.070	0.017	−5	9
SN 2000dm	Sab	0.185	0.015	−4	−5
SN 2000dn	S0	0.048	0.032	−26	15
SN 2000dr	S0	0.021	0.019	21	−6
SN 2000fa	Sd/Irr	0.067	0.021	7	−4
SN 2001C	Sb	0.070	0.011	15	−6
SN 2001E	Sc	0.039	0.019	1	−23
SN 2001V	Sb	0.020	0.015	52	28
SN 2001ah	Sbc	0.013	0.058	−4	−32
SN 2001ay	Sb	0.019	0.030	−10	9
SN 2001bf	. . .	0.099	0.015	5	−8
SN 2001bg	Sb	0.039	0.007	22	−19
SN 2001bp	. . .	0.023	0.095	4	−6
SN 2001br	Sa	0.065	0.021	2	2
SN 2001cj	Sb	0.014	0.024	−8	35
SN 2001ck	Sb	0.013	0.035	−6	3
SN 2001cp	Sbc	0.157	0.022	−49	−40
SN 2001da	Sab	0.058	0.017	9	−3
SN 2001dl	Sd/Irr	0.054	0.021	−2	11
SN 2001eh	Sb	0.064	0.037	−36	6
SN 2001en	Sd/Irr	0.054	0.016	6	−3
SN 2001ep	Sb	0.047	0.013	10	−16
SN 2001ex	Sb	0.053	0.026	−5	0
SN 2001fh	Sb	0.746	0.013	1	−6
SN 2002G	E	0.013	0.034	6	−7
SN 2002aw	Sb	0.007	0.026	−2	2
SN 2002bf	Sb	0.011	0.024	1	4
SN 2002bo	Sa	0.025	0.004	12	−14
SN 2002cd	Sbc	0.405	0.010	10	10
SN 2002cf	E	0.036	0.015	−16	9
SN 2002cr	Scd	0.025	0.009	41	50
SN 2002cs	E	0.108	0.016	25	−1
SN 2002cu	E	0.063	0.023	−91	−26
SN 2002cx	. . .	0.032	0.024	11	−18
SN 2002de	Sd/Irr	0.019	0.028	−4	1
SN 2002dj	E	0.095	0.009	−9	−3
SN 2002dl	Sc	0.078	0.016	10	−9
SN 2002do	E	0.314	0.016	0	8
SN 2002dp	Sc	0.049	0.012	31	22
SN 2002eb	Sb	0.061	0.028	−15	−14

Table 9
(Continued)

SN	Host	$E(B-V)_{\rm MW}$ (mag)	$z_{\rm helio}$	E (″)	N (″)
SN 2002ef	S0	0.032	0.024	10	7
SN 2002el	S0	0.087	0.029	−8	25
SN 2002er	Sa	0.161	0.009	−12	5
SN 2002eu	. . .	0.045	0.038	11	12
SN 2002fb	E	0.089	0.016	−18	−9
SN 2002fk	Sbc	0.040	0.007	−12	−4
SN 2002ha	Sab	0.102	0.014	−7	−29
SN 2002he	E	0.040	0.025	−20	−37
SN 2002jg	Sb	0.066	0.016	−20	−13
SN 2003D	E	0.065	0.022	2	−10
SN 2003W	Sc	0.048	0.020	0	3
SN 2003Y	S0	0.048	0.017	−4	19
SN 2003cg	Sa	0.031	0.004	14	5
SN 2003cq	Sbc	0.020	0.033	32	−2
SN 2003du	Sd/Irr	0.010	0.006	−9	−14
SN 2003fa	Sb	0.039	0.039	−10	49
SN 2003gn	Sab	0.050	0.034	16	−11
SN 2003gq	Sbc	0.069	0.021	−5	11
SN 2003gs	S0	0.035	0.005	13	−15
SN 2003gt	Sab	0.110	0.016	5	−5
SN 2003he	Sbc	0.039	0.025	−2	6
SN 2003hv	S0	0.015	0.006	17	−57
SN 2003kf	Sb	0.313	0.007	9	−14
SN 2004E	E/S0	0.015	0.030	3	20
SN 2004S	Sc	0.100	0.009	−47	−31
SN 2004as	Sd/Irr	0.015	0.031	0	−9
SN 2004at	. . .	0.012	0.023	−13	0
SN 2004bd	Sa	0.024	0.009	−2	−4
SN 2004bg	Sb	0.022	0.021	14	7
SN 2004bk	Sb	0.025	0.023	−10	−5
SN 2004br	E	0.023	0.023	−9	−1
SN 2004bv	Sbc	0.063	0.011	−4	−21
SN 2004bw	Scd	0.141	0.021	22	−7
SN 2004dt	Sa	0.027	0.020	7	11
SN 2004ef	Sb	0.055	0.031	−7	−9
SN 2004eo	Sab	0.108	0.016	59	7
SN 2004ey	Sc	0.137	0.016	8	−13
SN 2004fz	Sc	0.061	0.017	−2	−13
SN 2004gs	S0	0.031	0.027	−10	−13
SN 2005M	Sb	0.031	0.022	−7	−11
SN 2005am	Sa	0.054	0.008	18	31
SN 2005bc	Sb	0.010	0.012	5	8
SN 2005bl	E	0.029	0.024	13	−11
SN 2005bo	Sab	0.046	0.014	−8	−13
SN 2005cc	Sd/Irr	0.007	0.008	−1	−5
SN 2005cf	S0	0.097	0.006	−15	123
SN 2005de	Sb	0.102	0.015	−17	33
SN 2005dm	E	0.026	0.017	7	2
SN 2005el	S0	0.114	0.015	39	−23
SN 2005eq	Scd	0.074	0.029	16	26
SN 2005eu	. . .	0.131	0.035	−1	−1
SN 2005na	Sa	0.078	0.026	−2	−7
SN 2006D	Sab	0.046	0.009	−13	6
SN 2006X	Sbc	0.026	0.005	−12	−48
SN 2006ac	Sb	0.016	0.023	4	22
SN 2006bt	S0a	0.050	0.032	−44	−23
SN 2006cp	Sc	0.026	0.022	20	−15
SN 2006dm	Sc	0.039	0.022	8	−6
SN 2006ef	S0	0.024	0.018	8	25
SN 2006ej	Sc	0.035	0.020	−6	−5
SN 2006em	E	0.059	0.019	21	−51
SN 2006en	Sc	0.064	0.032	11	−4
SN 2006eu	E	0.194	0.024	13	−9
SN 2006gr	Sb	0.085	0.035	−23	−24
SN 2006hb	E	0.027	0.015	9	18
SN 2006je	Sb	0.046	0.038	19	21

Table 9
(Continued)

SN	Host	$E(B-V)_{\mathrm{MW}}$ (mag)	z_{helio}	E ($''$)	N ($''$)
SN 2006le	Sb	0.449	0.017	−12	40
SN 2006lf	Sb	0.954	0.013	13	−12
SN 2007O	Sc	0.023	0.036	8	−2
SN 2007af	Scd	0.039	0.005	−40	−22
SN 2007au	S0	0.067	0.021	41	−31
SN 2007bc	Sa	0.022	0.021	−29	−16
SN 2007bj	E	0.118	0.017	4	2
SN 2007ca	Sc	0.067	0.014	25	−2
SN 2007ci	E	0.026	0.018	−4	−12
SN 2007co	...	0.113	0.027	8	−15
SN 2007cq	...	0.109	0.026	−3	6
SN 2007fr	...	0.061	0.051	6	−34
SN 2007hj	S0	0.088	0.014	−7	14
SN 2007le	Sc	0.033	0.007	−4	−17
SN 2007qe	...	0.038	0.024	12	1
SN 2007sr	Sd/Irr	0.047	0.005	−3	−379
SN 2007ux	...	0.045	0.031	4	5
SNF20071021-000	...	0.069	0.028	−3	7
SN 2008A	Sa	0.054	0.016	−15	19
SN 2008C	S0a	0.084	0.017	−3	0
SN 2008L	S0	0.159	0.019	−6	−10
SN 2008Q	S0	0.083	0.008	141	42
SN 2008Z	...	0.012	0.021	−2	−7
SN 2008ar	Sa	0.037	0.026	5	3
SN 2008bf	E	0.035	0.024	20	46
SN 2008cl	S0	0.021	0.063	3	8
SN 2008dr	Sb	0.043	0.041	−1	8
SN 2008dt	S0a	0.046	0.035	1	−6
SN 2008dx	E	0.010	0.023	−45	−3
SN 2008ec	Sa	0.069	0.016	14	−7
SN 2008ei	Sd/Irr	0.085	0.038	−5	−3
SNF20080514-002	S0	0.034	0.022	−11	−12
SNF20080909-030	...	0.069	0.032	...	...

Note. SN offsets from the host-galaxy nucleus are given.

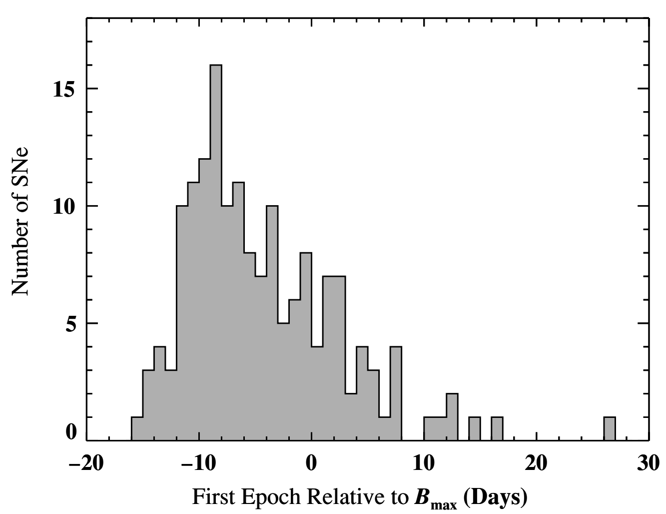

Figure 14. Distribution of first photometry epoch relative to B_{max}. The median value for our sample is 6 days before B_{max}.

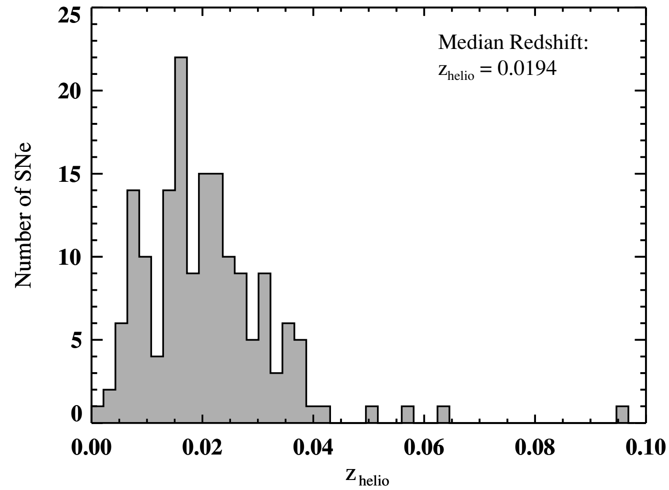

Figure 15. Redshift distribution for the LOSS sample. We find a median recession velocity of $cz_{\mathrm{helio}} = 5816$ km s^{-1} ($z_{\mathrm{helio}} = 0.0194$) for our sample.

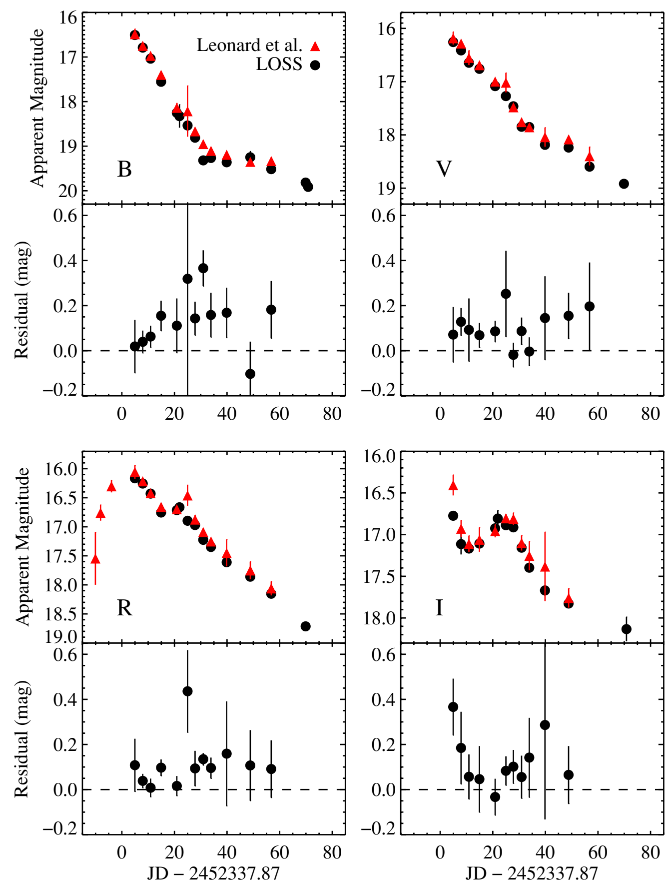

Figure 16. Comparison SN 2002bf photometry presented by Leonard et al. (2005) and by LOSS using the same KAIT data. SN 2002bf was only 4$''$.1 from the host-galaxy nucleus, providing an extreme test for our galaxy subtraction pipelines. The LOSS photometry is roughly 0.1 mag fainter in all bands. The first three R-band epochs from Leonard et al. (2005) are unfiltered observations which are not included in the LOSS photometry.

VRI measurements agree to within 0.03 mag while *B* is within 0.04 mag.

4.2.4. SN 2003du

Stanishev et al. (2007) present extensive *UBVRI* photometry of SN 2003du in the nearby galaxy UGC 09391. Our *BVRI* light curves start around B_{max}, about 10 days after those of Stanishev et al. Overall, the agreement between the two data sets is excellent. We share over 20 epochs in common and find that our light curves are within 0.03 mag in *BVR* and 0.05 mag in *I*. The light curves from Stanishev et al. are *S*-corrected, perhaps explaining the measured difference in the *I* band.

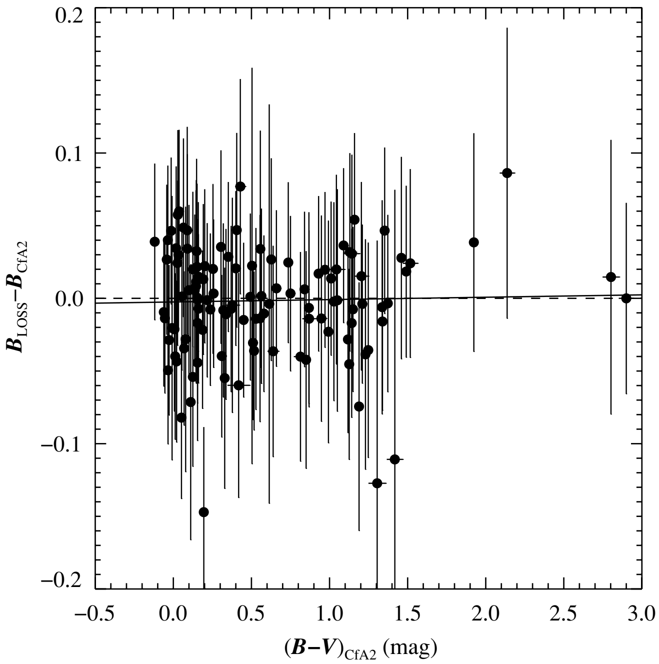

Figure 17. Residuals for overlapping LOSS and CfA2 data points as a function of $B-V$ color. A linear fit (solid line) to the data shows that there is not a strong relationship between the residuals and color, an indication that *S*-corrections will not substantially improve the agreement between data points.

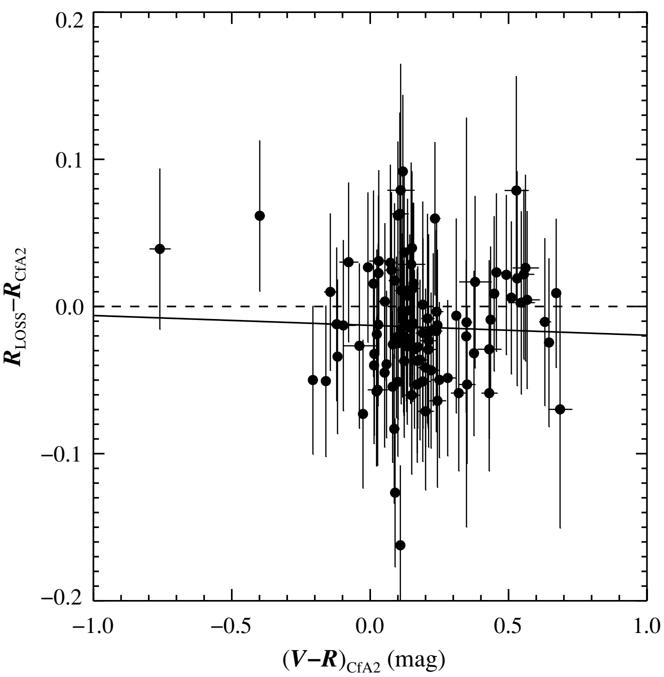

Figure 18. Residuals for overlapping LOSS and CfA2 data points as a function of $V-R$ color. A linear fit (solid line) to the data shows little to no relationship between residuals and color. A systematic shift of $\sim$0.01 mag accounts for the difference.

Anupama et al. (2005) also present optical photometry of SN 2003du, and we share $\sim$30 overlapping epochs. Our *BVR* light curves are systematically brighter by $\sim$0.05 mag while *I* is in excellent agreement to within 0.01 mag. The discrepancy in *BVR* between the two reductions can be traced back to calibrations for the local field standards. There are four overlapping comparison stars which we measure to be

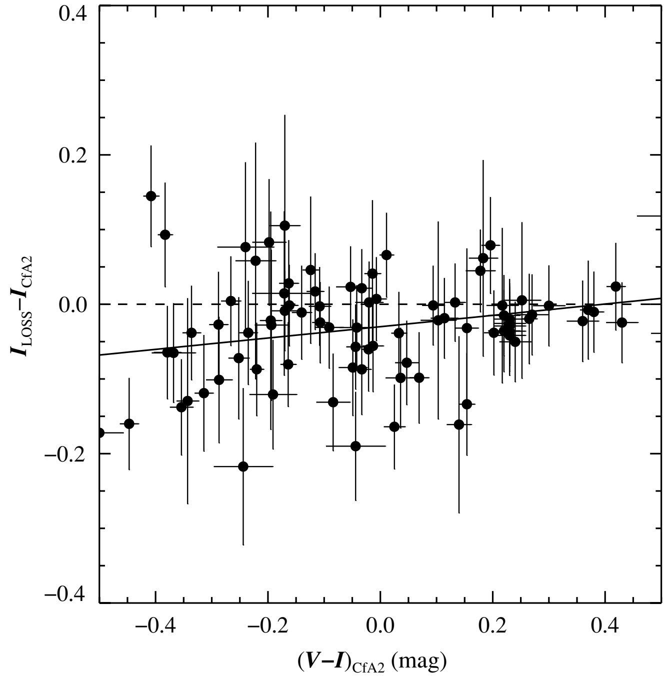

Figure 19. Residuals for overlapping LOSS and CfA2 data points as a function of $V-I$ color. A linear fit (solid line) to the data shows a correlation between the residuals and color, indicating that an *S*-correction could possibly improve the agreement between these two photometric data sets. Correcting for the linear fit reduces the scatter by 0.01 mag.

systematically brighter by $\sim$0.05 mag, once again underscoring the importance of consistent calibrations.

4.2.5. *CfA3*

The most recent release from the Center for Astrophysics, CfA3, roughly doubles the number of published nearby SN Ia light curves (Hicken et al. 2009b). CfA3 data obtained during 2001–2004 were taken in *UBVRI*, while subsequent data were in $UBVr'i'$. We share 69 SNe in common with CfA3. Combining the two data sets gives close to 260 SNe Ia with well-sampled light curves which could be used for cosmology. In this section, we compare the LOSS data set with the CfA3 data set, the two largest existing samples of nearby SNe Ia, to study any trends that arise. We include a systematic error of 0.02 mag for CfA3 data as suggested by Hicken et al. (2009b).

Similar to our comparison with CfA2, we compare individual CfA3 points with a linear interpolation to adjacent LOSS points that are within 4 days of one another. Of the 69 SNe in common, we can compare 67 *BV* light curves and 33 *RI* light curves. Table 11 provides the error-weighted mean residuals for individual SNe. To study the residuals in more detail, we plot the residuals for all of our data-point comparisons as a function of SN phase in Figure 20. Ideally, if we are not plagued by systematic errors from differences in calibrations or galaxy subtraction, we expect the mean residual to be $\sim$0 mag with a reasonable scatter ($\sigma \approx 0.05$ mag). We find the mean residual in *B* to be -0.013 mag with $\sigma = 0.114$ mag, in *V* to be 0.010 mag with $\sigma = 0.094$ mag, in *R* to be -0.014 mag with $\sigma = 0.071$ mag, and in *I* to be 0.018 mag with $\sigma = 0.074$ mag (see Table 12). This rather high level of scatter is fairly troubling considering that the sample is of bright, nearby SNe Ia. If we limit our comparison to data points brighter than mag 18, the scatter in all bands is reduced to a more reasonable $\sigma \approx$ 0.06–0.07 mag (see Table 13 for details), implying that the

Table 10
Photometric Comparison with CfA2

SN	*B* Residual	rms	*N*	*V* Residual	rms	*N*	*R* Residual	rms	*N*	*I* Residual	rms	*N*
SN 1998dh	−0.003 ± 0.022	0.023	7	−0.022 ± 0.022	0.009	7	0.032 ± 0.022	0.025	6	−0.044 ± 0.022	0.066	7
SN 1998dm	−0.021 ± 0.037	0.016	4	−0.010 ± 0.037	0.030	4	0.060 ± 0.037	0.029	4	0.036 ± 0.037	0.065	4
SN 1998ef	0.001 ± 0.027	0.045	4	−0.035 ± 0.027	0.026	4	−0.074 ± 0.027	0.043	4	−0.099 ± 0.027	0.031	4
SN 1998es	0.010 ± 0.023	0.049	7	−0.043 ± 0.023	0.050	7	−0.004 ± 0.023	0.044	9	−0.126 ± 0.023	0.049	6
SN 1999aa	0.024 ± 0.021	0.022	8	−0.036 ± 0.021	0.037	8	−0.050 ± 0.021	0.011	4	−0.003 ± 0.021	0.107	5
SN 1999ac	−0.005 ± 0.022	0.021	8	−0.041 ± 0.022	0.012	8	−0.030 ± 0.022	0.025	8	0.030 ± 0.022	0.052	8
SN 1999by	0.001 ± 0.014	0.021	15	−0.022 ± 0.014	0.016	15	−0.048 ± 0.014	0.013	15	−0.023 ± 0.014	0.019	15
SN 1999cl	0.023 ± 0.027	0.028	7	0.019 ± 0.027	0.013	8	0.020 ± 0.027	0.028	6	0.105 ± 0.027	0.021	7
SN 1999dq	0.010 ± 0.013	0.019	18	−0.021 ± 0.013	0.027	19	−0.003 ± 0.013	0.023	20	−0.001 ± 0.013	0.026	19
SN 1999ej	0.026 ± 0.044	0.008	2	0.001 ± 0.044	0.014	2	−0.009 ± 0.044	0.029	2	0.021 ± 0.044	0.035	2
SN 1999gh	−0.055 ± 0.058	0.025	2	0.038 ± 0.058	0.018	2	0.016 ± 0.058	0.010	2	0.111 ± 0.058	0.025	2
SN 1999gp	−0.061 ± 0.027	0.048	6	−0.018 ± 0.027	0.056	6	−0.045 ± 0.027	0.059	6	−0.006 ± 0.027	0.035	6
SN 2000cn	0.026 ± 0.021	0.049	12	0.036 ± 0.021	0.018	12	0.014 ± 0.021	0.032	12	0.032 ± 0.021	0.049	12
SN 2000dk	−0.033 ± 0.020	0.025	8	−0.001 ± 0.020	0.026	8	−0.018 ± 0.020	0.026	8	−0.095 ± 0.020	0.051	8
SN 2000fa	−0.016 ± 0.027	0.055	6	−0.009 ± 0.027	0.042	6	−0.019 ± 0.027	0.020	6	−0.108 ± 0.027	0.030	6

Note. The calculated mean residuals (mag) are LOSS minus CfA2.

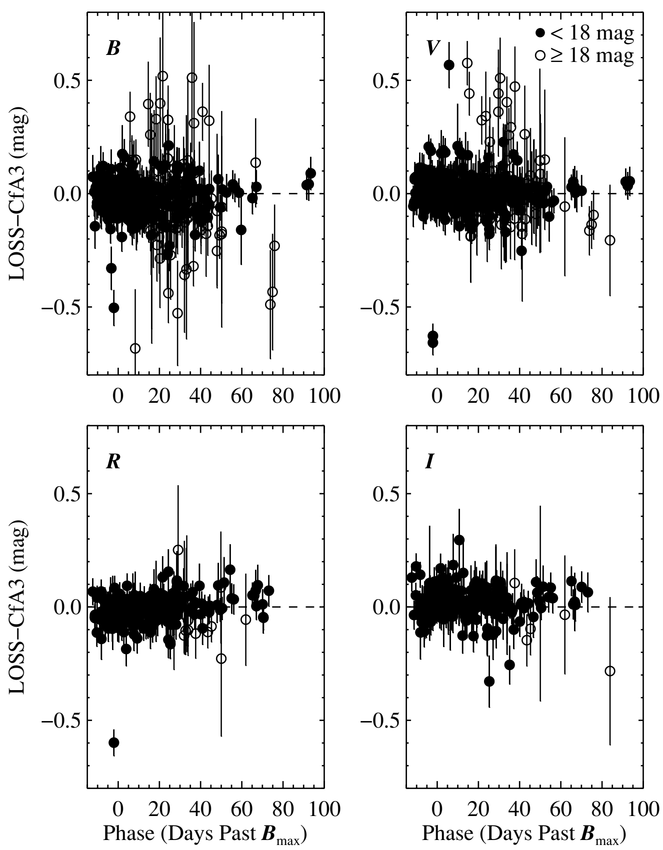

Figure 20. LOSS−CfA3 residuals for all comparison data points as a function of SN phase. Our data generally agree close to maximum light but grow discordant at late times. This is especially pronounced in *B* and *V*. If we restrict our comparison to points brighter than mag 18 (plotted in filled circles), we reduce the scatter significantly.

two groups have a decent level of agreement around maximum light. The disagreement at later phases could be caused by the increased importance of proper galaxy subtraction, the inherent difficulty in measuring faint objects, or the growing importance of *S*-corrections at late times as the spectral energy distribution of the SN becomes increasingly nonstellar.

While restricting our comparison to points brighter than mag 18 provides a significant improvement, the question now becomes whether this level of scatter is randomly distributed over all data points for all of the overlapping SNe, or is a result of systematic differences in individual SNe which could be introduced through improper galaxy subtraction or differences in field calibrations. In Figure 21, we construct a histogram of mean residuals as a function of the number of SNe. We code SN mean residuals computed with more than three data points with gray shading and mean residuals computed with three or fewer data points are unshaded. The only distribution which appears Gaussian is the *V* band, although there are clearly outliers which indicate SNe that suffer from a systematic offset. The *BI* histograms are not centered at 0 mag, while the *RI* histograms do not seem convincingly Gaussian.

The following SNe deserve special attention as being clear outliers: SN 2001V in *B* and SN 2006eu in *B* and *V*. For SN 2001V, the disagreement is tied to the differences in the local standard stars. We share two overlapping stars with CfA3 which we measure to be systematically fainter by 0.15 mag in *B*, thus explaining why we find the SN to be fainter by ∼0.13 mag in *B*. Surprisingly, comparing our local standards does not offer an explanation for the large discrepancies in SN 2006eu. We share four overlapping standards with CfA3 and we measure the stars to be fainter by ∼0.106 mag in *B* and brighter by 0.01 mag in *V*. This does not explain why LOSS measures SN 2006eu to be systematically fainter by 0.30 mag in *B* and 0.46 mag in *V*.

4.3. LOSS in the Wild

A few individual SN Ia light curves presented here have already been published in other papers. LOSS data for SN 2004eo reduced with the pipeline appeared in Pastorello et al. (2007) and data for SN 2002cx were supplied for Phillips et al. (2007). The LOSS reduction of SN 2002fk is in Riess et al. (2009) as a means to calibrate the SN distance ladder using Cepheid variables in NGC 1309. Data for SN 2003hv, reduced using our pipeline, were also presented by Leloudas et al. (2009).

5. DISCUSSION

A major goal in SN Ia science is to use their multi-color light curves to calibrate SNe Ia as cosmological distance indicators. As discussed in Section 3, this requires a large number of objects with well-sampled light curves that cover from before B_{max} to

Table 11
Photometric Comparison with CfA3

SN	*B* Residual	rms	*N*	*V* Residual	rms	*N*	*R* Residual	rms	*N*	*I* Residual	rms	N
SN 2001V	0.127 ± 0.028	0.040	9	−0.003 ± 0.025	0.044	11	0.102 ± 0.033	0.029	10	0.090 ± 0.029	0.018	7
SN 2001ah	...	...	0	0.101 ± 0.193	...	1	0.052 ± 0.124	0.130	4	...	...	0
SN 2001ay	−0.044 ± 0.037	0.055	5	−0.032 ± 0.027	0.010	8	−0.014 ± 0.027	0.021	8	0.053 ± 0.038	0.048	6
SN 2001bf	0.010 ± 0.021	0.013	7	0.008 ± 0.018	0.014	8	0.004 ± 0.019	0.013	8	0.007 ± 0.021	0.015	7
SN 2001cp	0.036 ± 0.066	...	1	−0.068 ± 0.036	0.125	3	−0.077 ± 0.035	0.109	3	−0.068 ± 0.063	0.266	2
SN 2001da	−0.009 ± 0.042	0.013	2	−0.067 ± 0.033	0.045	3	−0.082 ± 0.043	0.040	2	−0.019 ± 0.038	0.032	3
SN 2001eh	−0.012 ± 0.020	0.062	11	0.038 ± 0.017	0.038	13	−0.031 ± 0.017	0.025	12	−0.022 ± 0.023	0.111	11
SN 2001en	−0.040 ± 0.031	0.041	4	0.021 ± 0.027	0.023	4	−0.009 ± 0.028	0.011	4	0.056 ± 0.029	0.030	5
SN 2001ep	−0.031 ± 0.022	0.066	8	0.018 ± 0.016	0.022	12	0.007 ± 0.015	0.035	14	0.046 ± 0.017	0.016	12
SN 2001fh	−0.176 ± 0.043	0.268	3	−0.267 ± 0.025	0.360	5	−0.144 ± 0.029	0.302	4	−0.043 ± 0.030	0.017	4
SN 2002G	0.155 ± 0.215	...	1	−0.005 ± 0.097	...	1	−0.066 ± 0.082	...	1	0.086 ± 0.118	...	1
SN 2002bf	...	...	0	0.115 ± 0.062	...	1	0.019 ± 0.033	0.046	3	0.050 ± 0.041	0.133	5
SN 2002bo	−0.036 ± 0.018	0.066	12	−0.023 ± 0.017	0.027	10	−0.004 ± 0.015	0.048	14	0.024 ± 0.016	0.041	12
SN 2002cd	0.015 ± 0.037	0.057	5	−0.007 ± 0.026	0.028	5	−0.003 ± 0.026	0.014	5	0.081 ± 0.028	0.030	5
SN 2002cr	0.030 ± 0.019	0.021	8	0.001 ± 0.018	0.018	8	0.008 ± 0.018	0.032	8	−0.011 ± 0.018	0.023	8
SN 2002de	0.007 ± 0.028	0.011	4	0.059 ± 0.024	0.021	5	−0.042 ± 0.024	0.009	5	0.121 ± 0.029	0.036	5
SN 2002dj	−0.041 ± 0.017	0.012	12	0.018 ± 0.017	0.023	10	0.029 ± 0.019	0.037	8	0.090 ± 0.020	0.049	8
SN 2002do	0.038 ± 0.033	0.149	5	−0.025 ± 0.029	0.045	6	−0.012 ± 0.028	0.076	6	0.011 ± 0.027	0.027	7
SN 2002dp	−0.082 ± 0.023	0.059	7	−0.036 ± 0.018	0.056	10	−0.047 ± 0.020	0.035	9	0.038 ± 0.018	0.029	10
SN 2002eu	−0.067 ± 0.087	...	1	0.086 ± 0.068	...	1	−0.032 ± 0.044	0.004	2	0.027 ± 0.112	...	1
SN 2002fb	−0.105 ± 0.049	0.106	5	−0.009 ± 0.034	0.112	8	−0.042 ± 0.031	0.074	8	−0.014 ± 0.032	0.092	10
SN 2002fk	0.046 ± 0.020	0.052	8	0.019 ± 0.017	0.021	11	0.044 ± 0.015	0.029	15	0.015 ± 0.015	0.047	16
SN 2002ha	−0.031 ± 0.025	0.071	6	0.018 ± 0.024	0.030	6	0.011 ± 0.026	0.033	5	0.046 ± 0.024	0.038	6
SN 2002he	−0.021 ± 0.023	0.017	8	−0.045 ± 0.020	0.055	9	−0.052 ± 0.021	0.033	9	−0.093 ± 0.028	0.024	6
SN 2003D	...	...	0	−0.080 ± 0.154	0.073	2	−0.117 ± 0.110	...	1	0.106 ± 0.149	...	1
SN 2003W	0.021 ± 0.021	0.122	11	−0.029 ± 0.019	0.084	10	−0.005 ± 0.019	0.068	10	0.032 ± 0.019	0.062	14
SN 2003cg	0.013 ± 0.030	0.045	4	0.020 ± 0.022	0.012	6	0.007 ± 0.025	0.029	5	0.043 ± 0.026	0.025	4
SN 2003cq	...	...	0	−0.085 ± 0.061	0.131	3	−0.144 ± 0.060	0.139	3	...	...	0
SN 2003du	−0.001 ± 0.024	0.034	5	0.017 ± 0.015	0.022	12	−0.007 ± 0.013	0.026	18	0.017 ± 0.021	0.039	7
SN 2003fa	−0.067 ± 0.016	0.108	15	−0.008 ± 0.014	0.039	18	−0.063 ± 0.014	0.037	20	−0.041 ± 0.021	0.064	15
SN 2003kf	−0.041 ± 0.031	0.055	5	0.009 ± 0.028	0.019	4	−0.015 ± 0.027	0.015	4	0.001 ± 0.026	0.036	5
SN 2004as	−0.022 ± 0.036	0.017	3	−0.012 ± 0.027	0.040	6	−0.077 ± 0.026	0.048	6	−0.011 ± 0.036	0.034	6
SN 2004bg	−0.080 ± 0.027	0.110	7	−0.009 ± 0.019	0.038	11	−0.034 ± 0.020	0.041	10	−0.019 ± 0.042	0.021	3
SN 2004ef	−0.083 ± 0.041	0.167	3	−0.058 ± 0.033	0.055	5	...	...	0	...	...	0
SN 2005M	...	...	0	0.007 ± 0.041	0.006	2	...	...	0	...	...	0
SN 2005am	0.003 ± 0.015	0.082	16	−0.018 ± 0.013	0.033	18	...	...	0	...	...	0
SN 2005cf	0.017 ± 0.012	0.017	18	−0.020 ± 0.012	0.022	19	...	...	0	...	...	0
SN 2005el	−0.051 ± 0.018	0.061	17	0.026 ± 0.013	0.026	18	...	...	0	...	...	0
SN 2005eq	−0.084 ± 0.021	0.046	9	−0.046 ± 0.016	0.043	14	...	...	0	...	...	0
SN 2005eu	−0.089 ± 0.056	0.318	5	0.077 ± 0.021	0.154	15	...	...	0	...	...	0
SN 2005na	−0.109 ± 0.043	0.081	4	−0.060 ± 0.032	0.043	5	...	...	0	...	...	0
SN 2006D	−0.060 ± 0.054	0.081	2	0.038 ± 0.037	0.003	2	...	...	0	...	...	0
SN 2006X	0.081 ± 0.036	0.029	4	0.040 ± 0.023	0.049	7	...	...	0	...	...	0
SN 2006ac	−0.091 ± 0.065	0.180	2	−0.106 ± 0.071	0.063	2	...	...	0	...	...	0
SN 2006bt	−0.052 ± 0.036	0.045	9	−0.011 ± 0.031	0.063	10	...	...	0	...	...	0
SN 2006cp	−0.028 ± 0.036	0.034	5	−0.025 ± 0.039	0.024	4	...	...	0	...	...	0
SN 2006ef	0.041 ± 0.046	0.155	7	0.034 ± 0.042	0.054	5	...	...	0	...	...	0
SN 2006ej	0.055 ± 0.073	0.174	3	0.121 ± 0.040	0.101	3	...	...	0	...	...	0
SN 2006em	−0.483 ± 0.207	0.308	3	−0.078 ± 0.055	0.087	9	...	...	0	...	...	0
SN 2006en	−0.158 ± 0.039	0.151	6	−0.018 ± 0.034	0.041	7	...	...	0	...	...	0
SN 2006eu	0.285 ± 0.069	0.147	5	0.457 ± 0.043	0.118	9	...	...	0	...	...	0
SN 2006gr	−0.026 ± 0.021	0.018	9	−0.005 ± 0.019	0.033	10	...	...	0	...	...	0
SN 2006hb	...	...	0	−0.021 ± 0.021	0.036	13	...	...	0	...	...	0
SN 2006je	0.257 ± 0.126	0.156	3	0.000 ± 0.066	0.074	3	...	...	0	...	...	0
SN 2006le	−0.003 ± 0.017	0.034	15	0.029 ± 0.014	0.035	18	...	...	0	...	...	0
SN 2006lf	0.066 ± 0.025	0.065	13	−0.007 ± 0.017	0.070	18	...	...	0	...	...	0
SN 2007O	0.015 ± 0.045	0.173	3	0.088 ± 0.035	0.078	5	...	...	0	...	...	0
SN 2007af	0.008 ± 0.010	0.036	32	0.024 ± 0.011	0.021	23	...	...	0	...	...	0
SN 2007au	0.062 ± 0.027	0.098	8	0.029 ± 0.032	0.030	8	...	...	0	...	...	0
SN 2007bc	−0.032 ± 0.019	0.048	12	−0.008 ± 0.018	0.020	10	...	...	0	...	...	0
SN 2007ca	−0.104 ± 0.028	0.014	4	−0.065 ± 0.024	0.027	5	...	...	0	...	...	0
SN 2007ci	0.071 ± 0.024	0.034	7	0.065 ± 0.019	0.037	13	...	...	0	...	...	0
SN 2007co	−0.016 ± 0.014	0.052	20	0.021 ± 0.012	0.049	25	...	...	0	...	...	0
SN 2007cq	−0.015 ± 0.022	0.192	10	0.031 ± 0.017	0.081	12	...	...	0	...	...	0
SN 2007qe	0.027 ± 0.015	0.015	18	−0.001 ± 0.020	0.022	7	...	...	0	...	...	0
SN 2007sr	0.013 ± 0.013	0.022	19	−0.014 ± 0.015	0.026	12	...	...	0	...	...	0
SN 2008bf	−0.041 ± 0.020	0.096	15	0.173 ± 0.018	0.045	13	...	...	0	...	...	0

Note. The calculated mean residuals (mag) are LOSS minus CfA3.

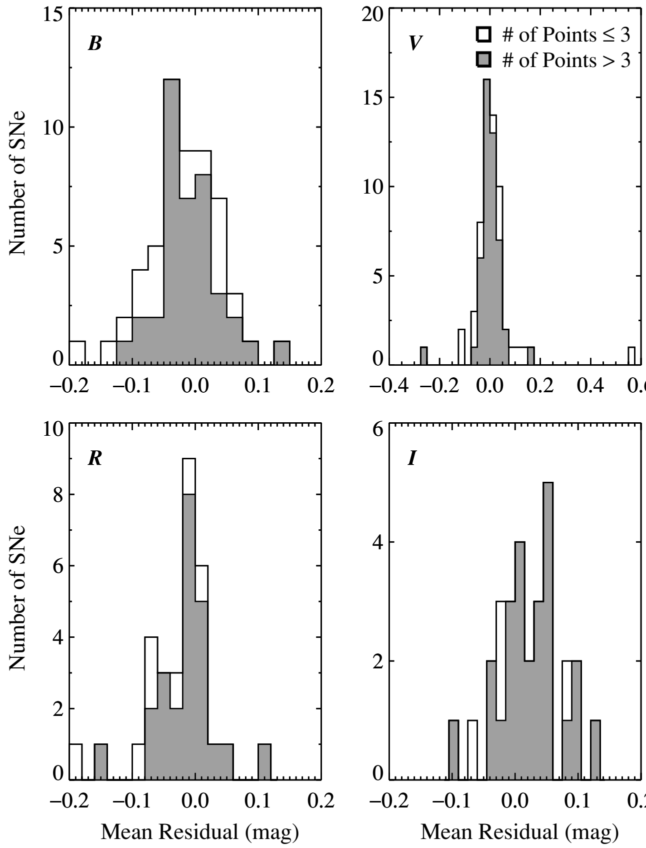

Figure 21. Histogram of the mean residual between CfA3 and LOSS data for individual SNe. Gray shading indicates SNe with mean residuals calculated using more than three points and mean residuals calculated with three or fewer points are unshaded. The asymmetric shape and offset from zero indicate systematic differences between individual SNe.

a month past. Our sample presents a self-contained data set which can be analyzed on its own and in comparison with other overlapping data sets to study the effects of systematics. In this section, we explore the properties of our light curves in more detail.

5.1. Light-curve Properties

The "width" of a light curve is an important parameter which has been shown to correlate very well with absolute peak brightness. One incarnation of this parameter is Δm_{15}, the difference between the SN magnitude at maximum light and 15 days past maximum light. We measure this quantity for both B and V using a template-fitting routine similar to that discussed by Prieto et al. (2006). We fit each band individually. Templates are constructed using light curves from our database that span the range of Δm_{15} and are well sampled. The data are K-corrected and corrected for Milky Way extinction (Schlegel et al. 1998). A fifth-order polynomial is fit to each template light curve to determine the date of maximum light. The light curves are shifted such that $t = 0$ is at maximum light and corrected for time dilation. Template light curves are constructed by fitting cubic splines between a range of −5 to 35 days past maximum light in each band. Lacking an SN 1991bg-like template, we augment our sample with the template of SN 1991bg from Prieto et al. (2006), which draws from photometry published by Hamuy et al. (1996c), Filippenko et al. (1992a), and Leibundgut et al. (1993). Our B templates are in the range $0.73 \leqslant \Delta m_{15} \leqslant 1.93$ mag and our V templates have $0.507 \leqslant \Delta m_{15} \leqslant 1.420$ mag.

Table 12
Summary of CfA3 Comparison Analyzed as an Ensemble

Filter	Mean (mag)	Standard Deviation	Error-weighted Mean
B	−0.016 ± 0.005	0.114	−0.009 ± 0.003
V	0.010 ± 0.004	0.094	0.006 ± 0.003
R	−0.014 ± 0.005	0.071	−0.015 ± 0.004
I	0.018 ± 0.005	0.074	0.022 ± 0.004

Note. The calculated mean residuals (mag) are LOSS minus CfA3.

Table 13
Summary of Bright CfA3 Comparison Analyzed as an Ensemble

Filter	Mean (mag)	Standard Deviation	Error-weighted Mean
B	−0.011 ± 0.006	0.069	−0.008 ± 0.003
V	0.006 ± 0.004	0.072	0.005 ± 0.003
R	−0.012 ± 0.005	0.067	−0.014 ± 0.004
I	0.021 ± 0.005	0.070	0.022 ± 0.004

Notes. The calculated mean residuals (mag) are LOSS minus CfA3. Only data points brighter than magnitude 18 are used.

We construct model light curves of varying Δm_{15} by taking linear combinations of our templates using the weighting scheme prescribed by Prieto et al. (2006) and calculating χ^2 to find the best fit. We use a triangle function to determine the weights of each template to construct models of varying Δm_{15}. For a given Δm^0_{15}, the weighting function is defined such that the triangle peaks at Δm^0_{15} (the extinction-corrected value of Δm_{15}) with a weight of 1 and falls symmetrically to 0 linearly over a range of Δm_{15} of width γ,

$$w_i = \begin{cases} 1 - \frac{2}{\gamma}\left|\Delta m_{15,i} - \Delta m^0_{15}\right| & \text{for } \left|\Delta m_{15,i} - \Delta m^0_{15}\right| \leqslant \gamma/2 \\ 0 & \text{for } \left|\Delta m_{15,i} - \Delta m^0_{15}\right| > \gamma/2. \end{cases}$$

Templates with $\Delta m_{15,i} > \Delta m^0_{15} + \gamma/2$ (that is, those templates that are the least like Δm^0_{15}) are suppressed from contributing to the model. The model for a light curve of width Δm^0_{15} in band X, $T^X(\Delta m^0_{15})$, is given by

$$T^X\left(\Delta m^0_{15}\right) = \frac{\sum_{i=0}^{N} w_i T_i^X}{\sum_{i=0}^{N} w_i},$$

where T_i is the template light curve associated with $\Delta m_{15,i}$ in band X. We increase γ with increasing values of Δm_{15} to reflect the sampling of Δm_{15} in our light-curve templates. The results are visually inspected to ensure that a good fit is obtained. In cases where Δm_{15} runs close to endpoints in the template range of Δm_{15} or we could not obtain a good fit, we instead fit a fifth-order polynomial to the data. The final results of our template and polynomial fits are presented in Tables 14. As a check on the reliability of our template fits, we compare the results between polynomial fitting and template fitting and find that they agree to within the error bars in instances where good fits can be obtained for both.

Figure 22 shows $\Delta m_{15}(B)$ plotted against $\Delta m_{15}(V)$. We only use SNe which have $\Delta m_{15}(B)$ and $\Delta m_{15}(V)$ whose template and polynomial fits agree to within the derived error bars, reducing our sample to 68. There is a clear monotonic relationship indicating that the decline rates in bands behave similarly. Using a nonlinear least-squares fitting routine, we fit a quadratic

Table 14
Summary of Bright CfA3 Comparison Analyzed as an Ensemble

SN	$t_{B_{\rm max}} - 2400000$	$B_{\rm max}$	$\Delta m_{15}(B)$	$t_{V_{\rm max}} - 2400000$	$V_{\rm max}$	$\Delta m_{15}(V)$	$(B - V)_{B_{\rm max}}$	Fit[a]
SN 1998dh	51029.35(0.50)	13.847(031)	1.227(033)	51031.25(0.50)	13.789(030)	0.658(033)	0.034(031)	T
SN 1998dm	51060.45(0.55)	14.680(033)	0.848(049)	51061.58(0.51)	14.377(031)	0.570(032)	0.303(034)	P
SN 1998ef	51113.60(0.51)	14.810(034)	1.303(046)	51115.16(0.51)	14.864(033)	0.686(042)	−0.072(037)	T
SN 1998es	51143.79(0.51)	13.749(037)	0.978(032)	51144.30(0.51)	13.691(036)	0.575(033)	0.056(042)	T
SN 1999ac	51249.44(0.51)	14.051(032)	1.182(033)	51252.01(0.52)	14.054(031)	0.607(033)	−0.038(033)	P
SN 1999by	51308.21(0.50)	13.576(032)	1.899(031)	51310.90(0.50)	13.089(031)	1.259(030)	0.412(032)	T
SN 1999cl	51341.84(0.50)	14.882(031)	1.144(032)	51343.86(0.50)	13.735(031)	0.665(034)	1.123(032)	T
SN 1999cp	51363.83(0.50)	13.918(030)	1.028(032)	51364.65(0.50)	13.960(031)	0.613(032)	−0.047(031)	T
SN 1999da	51369.80(0.53)	16.570(034)	1.975(062)	51372.55(0.52)	16.020(031)	1.211(054)	0.450(039)	P
SN 1999dg	51393.26(0.62)	15.907(037)	1.414(112)	51395.30(0.59)	15.956(037)	0.815(064)	−0.083(043)	T
SN 1999dk	51415.02(0.52)	14.754(034)	1.154(034)	51416.74(0.53)	14.730(034)	0.651(050)	0.003(037)	T
SN 1999dq	51436.45(0.50)	14.367(031)	0.961(031)	51437.66(0.50)	14.316(030)	0.527(032)	0.040(032)	T
SN 1999ej	51483.74(0.52)	15.355(031)	1.582(034)	51485.10(0.50)	15.389(030)	0.832(035)	−0.050(031)	T
SN 1999gp	51550.99(0.54)	15.930(031)	0.908(040)	51552.24(0.52)	15.976(031)	0.534(034)	−0.056(032)	T
SN 2000cn	51707.39(0.51)	16.526(032)	1.680(055)	51708.83(0.50)	16.444(031)	0.846(033)	0.063(033)	T
SN 2000cu	51744.68(0.51)	15.877(034)	1.563(036)	51746.11(0.51)	15.887(031)	0.777(034)	−0.027(034)	T
SN 2000cw	51748.55(0.50)	16.651(031)	1.310(037)	51750.29(0.51)	16.702(031)	0.669(035)	−0.072(031)	T
SN 2000cx	51752.27(0.50)	13.036(030)	0.960(032)	51754.45(0.52)	12.967(030)	0.835(031)	−0.952(031)	P
SN 2000dk	51812.68(0.50)	15.260(031)	1.718(041)	51813.96(0.50)	15.322(031)	0.888(038)	−0.079(032)	T
SN 2000dm	51816.39(0.57)	14.995(036)	1.562(051)	51817.46(0.51)	15.093(030)	0.803(036)	−0.111(037)	T
SN 2000dn	51824.80(0.51)	16.569(033)	1.115(032)	51826.65(0.52)	16.642(033)	0.643(079)	−0.092(036)	T
SN 2000dr	51833.98(0.54)	15.932(033)	1.744(037)	51836.40(0.52)	15.867(031)	0.961(037)	0.019(033)	T
SN 2000fa	51891.47(0.54)	15.827(033)	0.910(034)	51893.38(0.67)	15.803(035)	0.566(048)	0.007(037)	T
SN 2001bf	52045.32(0.50)	14.642(031)	0.933(032)	52045.95(0.52)	14.695(032)	0.529(045)	−0.058(034)	T
SN 2001br	52053.02(0.55)	16.235(032)	1.346(058)	52054.43(0.55)	16.147(031)	0.776(038)	0.067(033)	T
SN 2001cj	52066.04(0.53)	15.802(031)	0.965(034)	52067.33(0.52)	15.935(031)	0.562(036)	−0.141(032)	T
SN 2001ck	52073.02(0.70)	16.693(039)	1.058(122)	52073.98(0.59)	16.771(034)	0.595(067)	−0.085(044)	P
SN 2001cp	52089.26(0.53)	15.602(032)	0.915(040)	52089.89(0.51)	15.634(031)	0.575(032)	−0.035(033)	T
SN 2001da	52107.72(0.53)	15.482(032)	1.230(046)	52109.89(0.51)	15.325(031)	0.655(043)	0.130(032)	T
SN 2001dl	52131.47(0.53)	16.833(034)	0.981(035)	52132.38(0.51)	16.590(031)	0.585(032)	0.239(034)	T
SN 2001eh	52168.93(0.56)	16.556(032)	0.811(042)	52171.01(0.54)	16.656(031)	0.504(034)	−0.110(033)	P
SN 2001en	52193.02(0.50)	15.009(031)	1.274(044)	52194.24(0.50)	15.046(031)	0.688(035)	−0.050(031)	T
SN 2001ep	52199.85(0.50)	14.839(030)	1.356(034)	52201.71(0.50)	14.833(030)	0.680(034)	−0.019(031)	T
SN 2002G	52299.52(0.91)	17.621(039)	1.384(116)	52302.21(0.74)	17.323(048)	0.825(067)	0.243(054)	T
SN 2002bo	52357.50(0.52)	13.924(041)	1.194(053)	52359.20(0.52)	13.526(034)	0.702(036)	0.374(044)	T
SN 2002cd	52383.66(0.67)	15.574(034)	0.794(034)	52386.40(0.58)	14.941(034)	0.526(060)	0.601(037)	T
SN 2002cf	52384.90(0.55)	16.639(036)	1.864(064)	52387.12(0.56)	16.244(042)	1.160(036)	0.353(047)	T
SN 2002cr	52408.83(0.51)	14.160(031)	1.229(034)	52410.22(0.52)	14.206(031)	0.646(042)	−0.061(032)	T
SN 2002cs	52409.64(0.52)	15.047(033)	1.029(048)	52411.55(0.51)	15.096(032)	0.534(037)	−0.066(034)	T
SN 2002cu	52416.60(0.50)	16.097(032)	1.433(036)	52418.21(0.50)	16.090(031)	0.768(033)	−0.016(033)	T
SN 2002de	52433.61(0.50)	16.653(030)	0.996(031)	52435.20(0.51)	16.595(031)	0.562(033)	0.043(031)	T[a]
SN 2002dj	52450.74(0.50)	13.903(031)	1.087(032)	52452.63(0.51)	13.828(032)	0.668(041)	0.053(033)	T
SN 2002dl	52452.57(0.50)	15.780(031)	1.808(031)	52454.30(0.50)	15.677(030)	0.930(046)	0.077(031)	T
SN 2002do	52442.69(1.44)	15.481(109)	1.708(159)	52445.47(0.70)	15.507(032)	0.989(039)	−0.096(110)	T
SN 2002dp	52451.34(0.51)	14.452(031)	1.296(036)	52452.87(0.51)	14.427(031)	0.676(036)	0.009(033)	T
SN 2002eb	52494.59(0.50)	15.961(030)	0.987(030)	52496.14(0.50)	16.074(030)	0.531(031)	−0.125(031)	T
SN 2002ef	52491.51(0.57)	16.666(031)	1.040(104)	52492.65(0.51)	16.351(030)	0.630(048)	0.309(032)	T
SN 2002el	52508.76(0.50)	16.082(032)	1.390(037)	52510.03(0.50)	16.175(032)	0.729(034)	−0.107(034)	T
SN 2002er	52524.77(0.50)	14.174(031)	1.309(034)	52526.64(0.50)	14.066(031)	0.697(031)	0.084(031)	T
SN 2002fk	52548.15(0.50)	13.129(031)	1.075(031)	52548.84(0.51)	13.251(031)	0.607(032)	−0.123(031)	P
SN 2002ha	52581.43(0.51)	14.689(032)	1.355(047)	52582.64(0.50)	14.782(030)	0.770(031)	−0.104(033)	T
SN 2002he	52586.40(0.51)	16.183(035)	1.494(037)	52587.38(0.50)	16.224(032)	0.815(035)	−0.050(037)	T
SN 2002jg	52610.19(0.50)	17.150(032)	1.475(039)	52611.82(0.51)	16.538(031)	0.778(034)	0.589(033)	T
SN 2003W	52679.37(0.51)	15.874(032)	1.113(031)	52681.69(0.52)	15.745(032)	0.589(034)	0.096(034)	T
SN 2003Y	52676.59(0.59)	17.734(042)	1.727(093)	52679.26(0.51)	16.827(032)	1.234(043)	0.830(047)	P
SN 2003du	52766.13(0.55)	13.486(034)	0.950(031)	52766.86(0.59)	13.588(031)	0.556(032)	−0.106(034)	T
SN 2003fa	52807.53(0.50)	16.554(031)	0.956(030)	52808.48(0.50)	16.706(031)	0.515(031)	−0.160(031)	T
SN 2003gn	52853.09(0.55)	17.315(036)	1.243(082)	52854.59(0.50)	17.308(031)	0.737(032)	−0.011(037)	T
SN 2003gq	52848.41(0.61)	17.824(041)	1.693(188)	52852.50(0.63)	17.621(034)	1.013(067)	0.075(052)	P
SN 2003gt	52862.17(0.50)	14.887(031)	1.056(031)	52863.55(0.51)	14.895(032)	0.625(040)	−0.019(032)	T
SN 2003he	52876.46(0.51)	16.183(031)	0.987(032)	52878.22(0.52)	16.176(032)	0.560(035)	−0.010(033)	T
SN 2003hv	52892.67(0.52)	12.482(034)	1.637(037)	52893.12(0.63)	12.544(036)	0.868(034)	−0.065(040)	T
SN 2003kf	52980.36(0.58)	13.254(042)	0.873(082)	52981.19(0.53)	13.322(031)	0.507(030)	−0.080(042)	T
SN 2004as	53084.98(0.51)	16.912(034)	1.111(034)	53087.11(0.50)	16.865(031)	0.639(057)	0.021(034)	T
SN 2004at	53092.26(0.50)	15.641(030)	1.091(031)	53093.56(0.51)	15.807(032)	0.589(034)	−0.176(032)	T
SN 2004br	53146.96(1.60)	15.456(031)	0.683(155)	53151.68(0.63)	15.502(031)	0.636(044)	−0.097(046)	P

Table 14
(Continued)

SN	$t_{B_{\max}} - 2400000$	$B_{\max}$	$\Delta m_{15}(B)$	$t_{V_{\max}} - 2400000$	$V_{\max}$	$\Delta m_{15}(V)$	$(B-V)_{B_{\max}}$	Fit[a]
SN 2004bv	53161.01(0.50)	13.893(032)	0.888(040)	53162.14(0.51)	13.802(031)	0.527(036)	0.082(033)	T
SN 2004bw	53163.55(0.52)	15.758(032)	1.312(048)	53164.88(0.52)	15.823(031)	0.753(037)	−0.079(034)	T
SN 2004dt	53240.40(0.51)	15.155(032)	1.286(053)	53241.40(0.51)	15.228(032)	0.641(057)	−0.080(034)	T
SN 2004ef	53264.36(0.51)	16.823(032)	1.383(042)	53265.93(0.50)	16.756(031)	0.713(032)	0.048(033)	T
SN 2004eo	53278.34(0.50)	15.019(030)	1.390(031)	53280.16(0.50)	15.035(031)	0.685(037)	−0.042(031)	T
SN 2004ey	53304.30(0.55)	14.731(035)	0.963(056)	53305.09(0.60)	14.838(035)	0.573(044)	−0.110(039)	T
SN 2004fz	53333.87(0.50)	14.833(037)	1.399(050)	53335.71(0.50)	14.933(033)	0.718(033)	−0.127(039)	T
SN 2004gs	53356.34(0.51)	17.106(031)	1.775(036)	53358.41(0.53)	17.035(031)	0.692(072)	0.046(032)	T
SN 2005M	53405.90(0.55)	15.854(031)	0.827(039)	53407.49(0.61)	15.922(032)	0.507(049)	−0.082(032)	P
SN 2005am	53437.71(0.51)	13.679(032)	1.667(035)	53438.63(0.53)	13.607(031)	0.856(032)	0.065(034)	T
SN 2005bc	53470.58(0.52)	16.256(032)	1.394(046)	53471.72(0.51)	15.860(031)	0.799(037)	0.382(033)	T
SN 2005cf	53533.70(0.51)	13.254(032)	1.029(037)	53535.34(0.50)	13.252(031)	0.585(031)	−0.012(032)	T
SN 2005de	53598.85(0.50)	15.347(031)	1.220(034)	53600.33(0.50)	15.324(031)	0.615(035)	0.010(032)	T
SN 2005el	53647.08(0.51)	14.822(034)	1.309(053)	53647.98(0.50)	14.928(031)	0.764(032)	−0.114(035)	T
SN 2005eq	53654.90(0.51)	16.201(033)	0.882(045)	53655.80(0.52)	16.214(032)	0.514(032)	−0.021(034)	T
SN 2005eu	53660.57(0.52)	16.369(036)	0.938(038)	53661.18(0.51)	16.435(035)	0.742(043)	−0.072(040)	T
SN 2005na	53741.93(0.67)	15.905(037)	1.239(060)	53742.50(0.91)	16.030(036)	0.639(070)	−0.128(042)	T
SN 2006bt	53857.51(0.61)	16.924(036)	0.877(046)	53859.67(0.51)	16.756(031)	0.602(032)	0.146(037)	T
SN 2006cp	53897.07(0.61)	15.908(038)	0.993(050)	53899.23(0.55)	15.813(032)	0.660(064)	0.063(039)	T
SN 2006dm	53928.96(0.50)	15.982(032)	1.543(034)	53930.35(0.50)	15.987(032)	0.850(036)	−0.022(034)	T
SN 2006ef	53970.02(0.56)	15.530(033)	1.384(052)	53970.68(0.53)	15.519(031)	0.717(036)	0.004(034)	T
SN 2006ej	53976.28(0.64)	15.729(054)	1.397(154)	53977.95(0.58)	15.749(042)	0.770(048)	−0.046(062)	T
SN 2006eu	53987.35(0.85)	17.318(048)	1.309(144)	53987.03(0.79)	16.827(036)	0.707(051)	0.501(053)	P
SN 2006gr	54012.60(0.52)	16.843(045)	1.029(057)	54014.36(0.52)	16.863(038)	0.586(040)	−0.036(051)	T
SN 2006le	54047.85(0.62)	14.738(037)	0.888(048)	54049.46(0.52)	14.858(034)	0.548(037)	−0.134(040)	T
SN 2006lf	54045.21(0.54)	13.800(043)	1.308(084)	54046.26(0.56)	13.857(042)	0.783(045)	−0.068(052)	T
SN 2007af	54174.50(0.56)	13.103(034)	1.222(047)	54176.13(0.53)	13.099(032)	0.673(037)	−0.014(036)	T
SN 2007au	54184.18(0.51)	16.519(036)	1.806(037)	54185.76(0.57)	16.389(054)	0.936(070)	0.108(057)	T
SN 2007bc	54200.14(0.53)	15.803(034)	1.349(069)	54201.94(0.51)	15.898(031)	0.698(034)	−0.120(034)	T
SN 2007ci	54246.55(0.52)	15.914(039)	1.744(038)	54248.60(0.52)	15.877(034)	0.880(053)	0.003(042)	T
SN 2007co	54264.68(0.53)	16.436(032)	1.040(104)	54266.48(0.50)	16.426(030)	0.590(031)	−0.008(032)	T
SN 2007cq	54280.43(0.52)	15.820(032)	1.066(033)	54282.38(0.50)	15.852(030)	0.633(036)	−0.053(033)	T
SN 2007fr	54302.51(0.52)	18.061(036)	1.790(039)	54303.96(0.58)	18.136(041)	0.832(067)	−0.095(045)	T
SN 2007hj	54350.13(0.55)	15.542(034)	1.953(058)	54352.27(0.51)	15.419(031)	1.027(033)	0.090(038)	P
SN 2007le	54398.94(0.52)	13.859(034)	1.015(041)	54400.11(0.73)	13.572(036)	0.554(038)	0.280(039)	T
SN 2007qe	54429.07(0.50)	16.003(032)	1.035(038)	54431.20(0.61)	15.989(044)	0.554(043)	−0.011(045)	T
SNF20071021-000	54407.83(0.52)	16.443(031)	1.239(046)	54409.60(0.55)	16.489(032)	0.668(051)	−0.066(033)	T
SN 2007sr	54448.34(0.75)	12.713(045)	1.053(066)	54448.97(1.64)	12.628(071)	0.542(057)	0.081(078)	T
SN 2007ux	54464.98(1.61)	17.229(100)	1.744(073)	54467.16(0.89)	17.269(032)	0.841(069)	−0.076(101)	T
SN 2008Q	54506.26(0.50)	13.481(030)	1.250(084)	54507.37(0.50)	13.483(031)	0.757(038)	−0.012(031)	T
SN 2008Z	54515.81(0.54)	16.399(036)	0.910(059)	54516.78(0.63)	16.284(056)	0.554(048)	0.109(059)	T
SN 2008ar	54534.57(0.70)	16.228(042)	1.078(055)	54536.21(0.63)	16.314(037)	0.521(066)	−0.101(047)	T
SN 2008bf	54555.14(0.53)	15.672(036)	1.029(069)	54556.05(0.53)	15.874(033)	0.564(036)	−0.207(038)	T
SN 2008dt	54646.73(3.05)	18.068(119)	0.958(135)	54649.15(1.25)	17.523(040)	0.613(057)	0.514(122)	T
SN 2008ec	54674.28(0.55)	15.491(033)	1.362(065)	54676.12(0.53)	15.386(032)	0.722(040)	0.081(034)	T
SNF20080514-002	54613.01(0.53)	15.834(034)	1.386(042)	54613.90(0.53)	15.992(033)	0.779(039)	−0.167(037)	T

Notes. 1σ uncertainties (mag) including both statistical and systematic errors noted in parentheses. Those for $B_{\max}$, $\Delta m_{15}(B)$, $V_{\max}$, $\Delta m_{15}(V)$, and $(B-V)_{B_{\max}}$ are reported in units of 0.001 mag.
[a] (T)emplate or (P)olynomial fit.

polynomial to find our best fit by the functional form

$$\Delta m_{15}(V) = 0.17(\Delta m_{15}(B))^2 + 0.04(\Delta m_{15}(B)) + 0.36.$$

This fit has $\chi^2 = 225$ for 65 degrees of freedom. The scatter in the fit increases significantly for rapidly declining objects.

Figure 23 shows a histogram of the distribution of $(B - V)_{B_{\max}}$ values for our sample. We find a median value of $(B - V)_{B_{\max}} = -0.02$ mag. We further explore the distribution of $(B - V)_{B_{\max}}$ values by plotting them against $\Delta m_{15}(B)$ in Figure 24. We break our sample into three categories: SN 1991T-like, normal, and SN 1991bg-like. These categories are defined spectroscopically and are either taken from the literature or from running the SuperNova IDentification (SNID) code (Blondin & Tonry 2007) on our spectroscopic database; see J. M. Silverman et al. (2010, in preparation) for more details on our implementation of SNID to our spectroscopic database. SNe that are SN 1991T-like are characterized by a lack of Si II and Ca II in premaximum spectra, have broader lights curves, and are more luminous than the typical SNe Ia (Filippenko et al. 1992b; Phillips et al. 1992). Objects that are SN 1991bg-like show strong Ti II and weak Fe II features at maximum light, and are intrinsically underluminous compared with normal SNe Ia (Filippenko et al. 1992a; Leibundgut et al. 1993). For a general

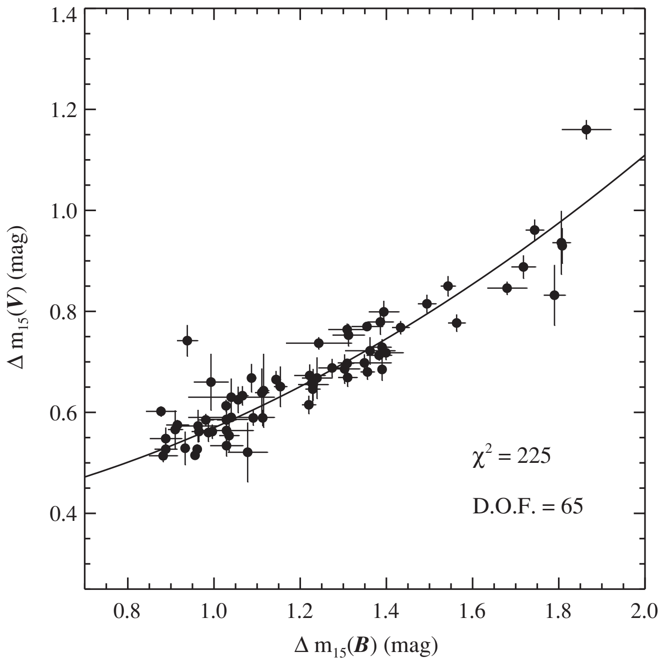

Figure 22. Measurements of $\Delta m_{15}(B)$ plotted against $\Delta m_{15}(V)$. We fit the data with a quadratic polynomial.

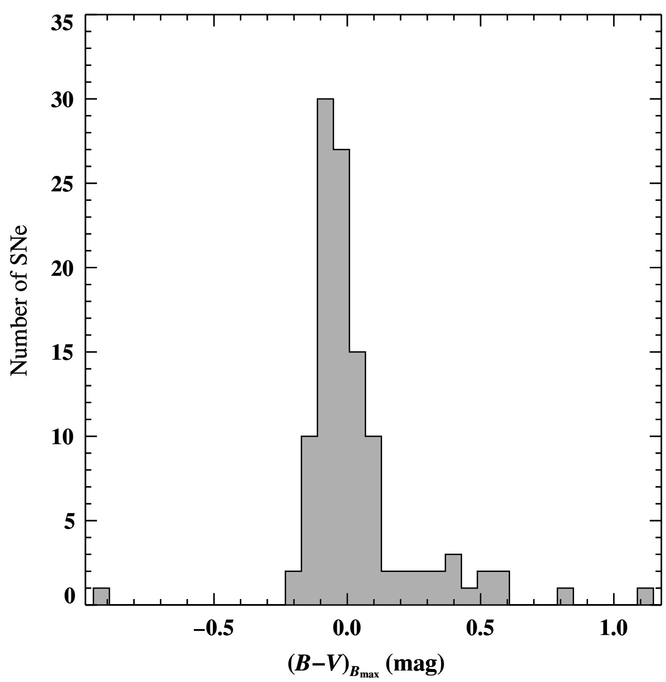

Figure 23. Distribution of $B - V$ values at $B_{\max}$. There is a clear peak at $B - V \approx 0$ mag with a tail that extends out to larger $B - V$ values. We find that SNe in the tail of the distribution are those that exhibit a significant amount of host-galaxy reddening and SN 1991bg-like objects. The bluest object that lies far to the left of the rest of the distribution in the peculiar SN 2000cx.

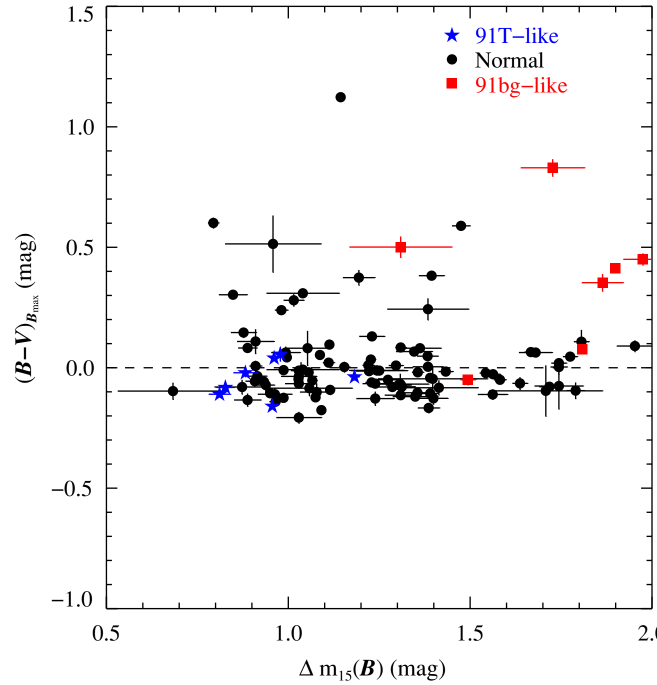

Figure 24. Comparison of $\Delta m_{15}(B)$ to $(B - V)_{B_{\max}}$. Objects have been coded by color and shape to highlight where different SN subclasses lie on the plot. SN 1991T-like objects are blue stars, normal SNe Ia are black circles, and SN 1991bg-like objects are red squares. Note that 5 of the 16 reddest objects are SN 1991bg-like.

review of the spectroscopic diversity of SNe Ia, see Filippenko (1997).

Of 18 SN 1991bg-like objects in our sample, we are able to measure Δm_{15} for 7. It is interesting to note that 5 of the 7 have $(B - V)_{B_{\max}} > 0.3$ mag. Of the 16 objects with $(B - V)_{B_{\max}} > 0.2$ mag, almost a third are SN 1991bg-like. Similar results have been presented by Garnavich et al. (2004) in the case of SN 1999by and Hicken et al. (2009b) for SN 1991bg-like rapid decliners in the CfA3 data set. The 9 SN 1991T-like SNe (including similar SN 1999aa-like objects (Krisciunas et al. 2000; Li et al. 2001b)) share an even tighter grouping of $(B - V)_{B_{\max}}$ values with an average of -0.055 mag. The 91 spectroscopically normal SNe Ia are mostly clustered a little below $(B - V)_{B_{\max}} \approx 0$ mag with a few exceptions. There are 11 SNe that have $(B - V)_{B_{\max}} \geqslant 0.2$ mag, hinting that they may suffer from significant host-galaxy extinction. Using MLCS2k2 to fit our light curves (see Section 5.2 for details), our suspicion is confirmed; MLCS2k2 finds that these SNe have $A_V \geqslant 0.4$ mag.

5.2. Late-time Colors

We have run the MLCS2k2.v006 distance fitter (Jha et al. 2007) on our data set. Following the path set by Hicken et al. (2009a), we have run MLCS2k2 using two sets of priors for host-galaxy extinction: $R_V = 3.1$ and $R_V = 1.7$. In a companion cosmology paper to follow (M. Ganeshalingam et al. 2010, in preparation), we will discuss the results of the two choices on the KAIT sample in more detail. For the purposes of this paper, in which we simply wish to characterize our data set, we will adopt the results of setting $R_V = 3.1$; using $R_V = 1.7$ does not affect the results below. For example, we find that the values derived for the MLCS2k2 Δ parameter for both sets of priors are within the 1σ errors for SNe with $A_V < 1.0$ mag. However, we do caution that there is a noticeable systematic trend between Δ residual and A_V (derived either using $R_V = 1.7$ or $R_V = 3.1$) which may slightly change the appearance of a few plots, but not the qualitative results presented below.

MLCS2k2 derives improved distances to SNe by parameterizing the absolute magnitude of an SN in the form of Δ, a measurement of how luminous an SN is compared to some fiducial value (with smaller Δ indicating an intrinsically brighter SN). This is done by attempting to separate intrinsic reddening

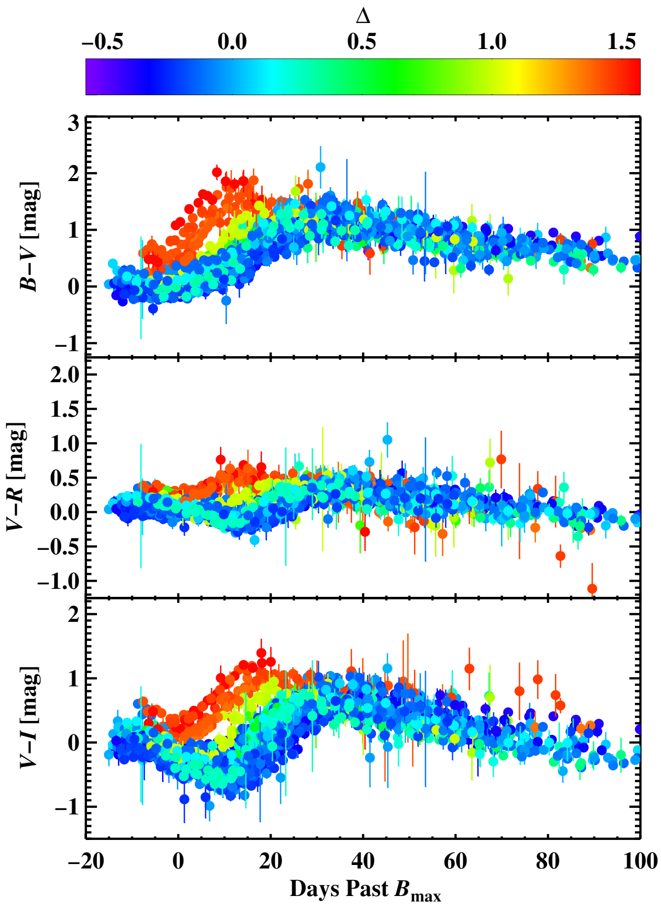

Figure 25. Color curves for 133 SNe from the LOSS sample color coded by the MLCS parameter Δ, which quantifies the width of the light curve in the sense that smaller Δ corresponds to a broader light curve. The top panel shows the $B - V$ color curve, the middle $V - R$, and the bottom $V - I$. The color curves have been shifted relative to maximum light in the B band and corrected for time dilation. All curves have been corrected for Milky Way reddening. We use only SNe that have $A_V \leqslant 1.0$ mag as found with MLCS. Despite SNe with various Δ values having very distinct color evolution for $t < 30$ days after B_{max}, there is a remarkable convergence to similar evolution in the interval 30 days $< t < 95$ days, mostly independent of Δ, as was first noted by Lira (1996). We measure an average slope that is in good agreement with the Lira–Phillips relation (Phillips et al. 1999).

in an SN from reddening from the host galaxy and then fitting to a training set of SN templates which are deemed to be free of host-galaxy extinction. Corrections for reddening are modeled as an intrinsic component governed by a Gaussian distribution of $B - V$ color 35 days past B_{max} that is uncorrelated with peak brightness and host-galaxy extinction given by a falling exponential peaking at $A_V = 0$ mag. The measured value of $(B - V)_{35}$ is drawn from the distribution formed by the convolution of the two different probability functions.

The explicit assumption is that the reddening can be disentangled into an intrinsic reddening component and a host-galaxy reddening component. Lira (1996) noted that the late-time $B-V$ color evolution for SNe with negligible host-galaxy extinction is strikingly similar, independent of $\Delta m_{15}(B)$. Phillips et al. (1999) used this observation to derive host-galaxy reddening estimates by determining the intrinsic late-time $B - V$ color behavior of four SNe in dust-free environments to correct the observed $B - V$ color of SNe that suffer from host-galaxy reddening. The authors measured an average slope of -0.0118 mag day^{-1} in the $B - V$ color curve in the interval 30 days $< t < 90$ days, which has come to be known as the Lira–Phillips law.

The LOSS sample offers a significantly larger sample with which to test the Lira–Phillips law. In Figure 25, we plot $B - V$, $V - R$, and $V - I$ color curves for 133 SNe from our sample color coded by the MLCS parameter Δ. Our sample excludes SNe which have an $A_V > 1.0$ mag as measured by MLCS. All light curves have been corrected for Milky Way extinction, K-corrected, corrected for time dilation, and shifted relative to the date of B_{max}. What starts out as a dissonant tidal wave of data points marking quite distinct evolution at early times, converges to a similar evolution in the range 30 days $< t <$ 90 days similar to the results found by Lira (1996), Phillips et al. (1999), and most recently Folatelli et al. (2010).

We measure $(B - V)_{35}$ for our sample by fitting a line with a fixed slope of -0.0118 mag day^{-1} to SNe with $B - V$ color curves having data at 30 days $< t <$ 90 days. We require that SNe have four or more data points in this range and are reliably fit. The results for 76 SNe from our sample can be found in Table 15. We also fit our $B - V$ color curves at this phase allowing the slope to vary. The error-weighted mean slope for our sample is -0.0115 ± 0.0001 mag day^{-1}, in excellent agreement with Phillips et al. (1999).

As was done by Jha et al. (2007), we fit a convolution of the two-component reddening model using a maximum-likelihood analysis. The parameters being fit are the peak and standard deviation (σ_{B-V}) of a Gaussian distribution of $(B - V)_{35}$ representing the intrinsic redness of SNe Ia at late times, and the scale length (τ_{B-V}) of a decaying exponential which models the probability distribution for host-galaxy reddening. The decaying exponential is truncated at the peak of the Gaussian to prevent negative-extinction measurements. To derive uncertainties for our fit, we performed a bootstrap analysis of the distribution.

Our results are shown in Figure 26. We find a mean $(B - V)_{35} = 1.006 \pm 0.022$ mag, $\sigma_{B-V} = 0.076 \pm 0.019$ mag, and $\tau_{B-V} = 0.161 \pm 0.036$ mag. Jha et al. find $(B - V)_{35} = 1.054 \pm 0.018$ mag, $\sigma_{B-V} = 0.062 \pm 0.012$ mag, and $\tau_{B-V} = 0.138 \pm 0.023$ mag using 82 objects, which mostly agree with the results presented here within the 1σ uncertainties. A Kolmogorov–Smirnoff test indicates that there is a 6% probability that the $(B-V)_{35}$ distribution presented here and that of Jha et al. (2007) are drawn from the same overall distribution. This rather small probability most likely reflects the different observational bias in each sample. The Lira–Phillips law as given by Phillips et al. (1999) predicts a mean $(B - V)_{35} \approx 1.044$ mag with a scatter of 0.05 mag. More recently, Folatelli et al. (2010) found an observed scatter about the Lira–Phillips law of 0.077 mag using a subset of the CSP sample with low host-galaxy reddening, although their analysis was done in the natural system of the Swope+CSP bands. Our values are in good agreement with these previously derived results.

Our larger value of τ is caused by the inclusion of SN 2006X and SN 1999cl, two SNe that appear to have extreme reddening properties. However, even with this value of τ, SNe having such extreme reddening are expected to be rare. Wang et al. (2009a) found both of these SNe to be members of a spectroscopic subclass that displayed a high-velocity Si II feature around maximum light in comparison with normal SNe Ia. On average, Wang et al. found that high-velocity SNe Ia are redder than spectroscopically normal SNe Ia and may be described by a different reddening distribution. While the prescription of a Gaussian convolved with a decaying exponential does a good

Table 15
Lira–Phillips Fits for $(B - V)_{35}$

SN	$(B - V)_{35}$	$\sigma(B - V)_{35}$
SN 1998dh	1.195	0.032
SN 1998dm	1.439	0.036
SN 1998ef	1.267	0.042
SN 1999aa	1.097	0.036
SN 1999ac	1.156	0.032
SN 1999cl	2.176	0.061
SN 1999dk	1.172	0.040
SN 1999dq	1.281	0.035
SN 1999ej	1.089	0.043
SN 1999gh	1.062	0.041
SN 2000cu	1.235	0.102
SN 2000cx	0.839	0.030
SN 2000dk	0.963	0.056
SN 2000dr	1.073	0.081
SN 2001V	1.245	0.040
SN 2001bf	1.087	0.036
SN 2001cj	1.012	0.058
SN 2001cp	0.967	0.085
SN 2001da	1.163	0.043
SN 2001dl	1.349	0.060
SN 2001en	1.132	0.040
SN 2001ep	1.278	0.040
SN 2002aw	1.257	0.047
SN 2002bf	1.307	0.045
SN 2002bo	1.407	0.031
SN 2002cr	1.138	0.032
SN 2002cu	1.113	0.060
SN 2002de	1.179	0.057
SN 2002dl	1.072	0.044
SN 2002dp	1.199	0.031
SN 2002eb	1.189	0.043
SN 2002er	1.282	0.037
SN 2002fk	1.069	0.032
SN 2002ha	0.967	0.036
SN 2002he	1.091	0.044
SN 2003du	1.028	0.030
SN 2003gs	1.063	0.032
SN 2003gt	1.224	0.033
SN 2003he	1.100	0.042
SN 2003hv	0.969	0.031
SN 2003kf	1.071	0.032
SN 2004S	1.000	0.036
SN 2004at	1.076	0.048
SN 2004bg	1.062	0.040
SN 2004bk	1.204	0.036
SN 2004bv	1.201	0.032
SN 2004bw	1.018	0.057
SN 2004dt	1.130	0.035
SN 2004ef	1.176	0.116
SN 2004eo	1.111	0.042
SN 2004ey	1.142	0.034
SN 2005M	1.053	0.037
SN 2005am	1.115	0.032
SN 2005bc	1.369	0.045
SN 2005cf	1.215	0.031
SN 2005de	1.222	0.038
SN 2005el	0.905	0.036
SN 2005eq	1.075	0.054
SN 2005eu	1.214	0.067
SN 2005na	1.016	0.045
SN 2006D	0.985	0.034
SN 2006X	2.334	0.040
SN 2006dm	0.906	0.050
SN 2006ef	1.083	0.042
SN 2006ej	1.063	0.050
SN 2006hb	1.055	0.048
SN 2007af	1.196	0.031
SN 2007bj	0.840	0.036
SN 2007co	1.108	0.054
SN 2007cq	1.050	0.038
SN 2007hj	1.117	0.041
SN 2007le	1.455	0.032
SN 2008A	1.424	0.047
SN 2008bf	1.061	0.043
SN 2008ec	1.320	0.045

Note. Units are magnitudes.

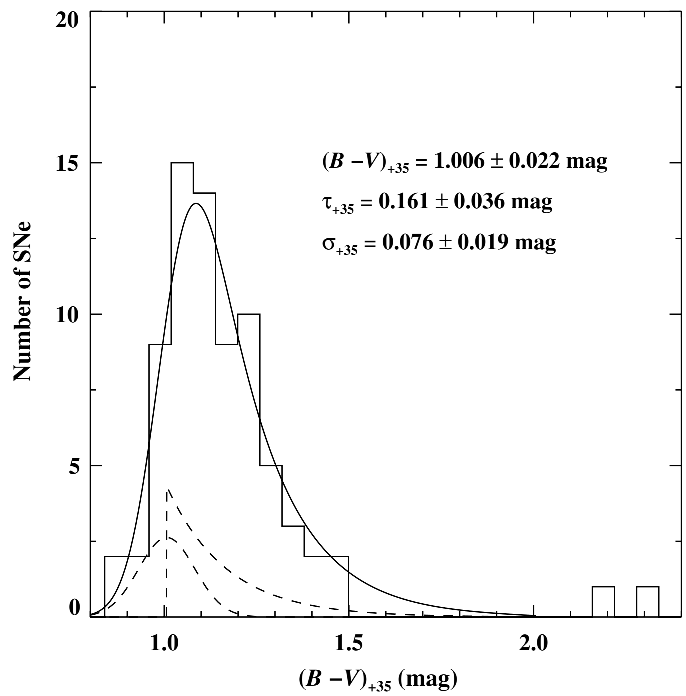

Figure 26. Distribution of $B - V$ values at 35 days past B_{max}. We fit a Gaussian convolved with a decaying exponential to the distribution to determine the intrinsic scatter in SN color at late times. An example of the two functions is shown with broken lines, although not to scale. The best-fit convolution of the two distributions is overplotted as a solid line.

job of modeling the late-time color distribution of most of our sample, it does not explain extremely reddened SNe such as SN 2006X and SN 1999cl.

The prescribed reddening treatment fails for the emerging class of SN 2002cx-like objects (Li et al. 2003b; Jha et al. 2006a; Phillips et al. 2007). As we have noted throughout this paper, since we manually select SNe Ia to monitor, there is no reason our sample should reflect the true population of SNe Ia, and we emphasize that the sample is most likely biased. For example, our sample may have a relative excess of bluer SNe Ia which are easier to discover and hence more likely to be selected for photometric monitoring.

5.3. Galaxy Distribution

Using Δ as a proxy for the absolute magnitude of an SN and thus its decline rate, we can break our sample into three sets: fast decliners ($\Delta > 0.3$), normal ($-0.15 \leqslant \Delta \leqslant 0.3$), and slow decliners ($\Delta < -0.15$). In Figure 27, we show a histogram of

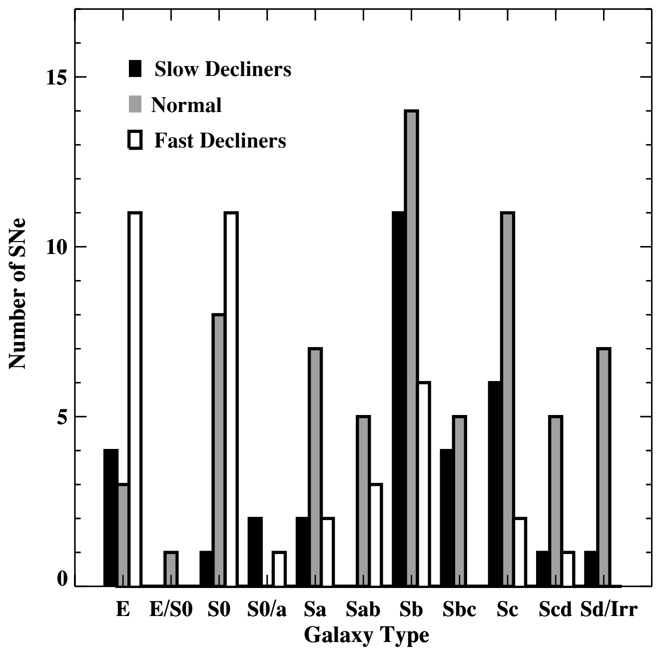

Figure 27. Histogram of galaxy morphologies for the LOSS sample broken up by decline rate. Dark shading indicates slow decliners, normal SNe Ia have gray shading, and fast decliners are unshaded. We define decline rates by using the MLCS2k2 parameter Δ. Slow decliners have $\Delta < -0.15$, normal SNe Ia have $-0.15 \leqslant \Delta \leqslant 0.3$, and fast decliners have $\Delta > 0.3$. Fast decliners in our sample are preferentially found in early-type galaxies, while normal SNe Ia and slow decliners are in later-type galaxies.

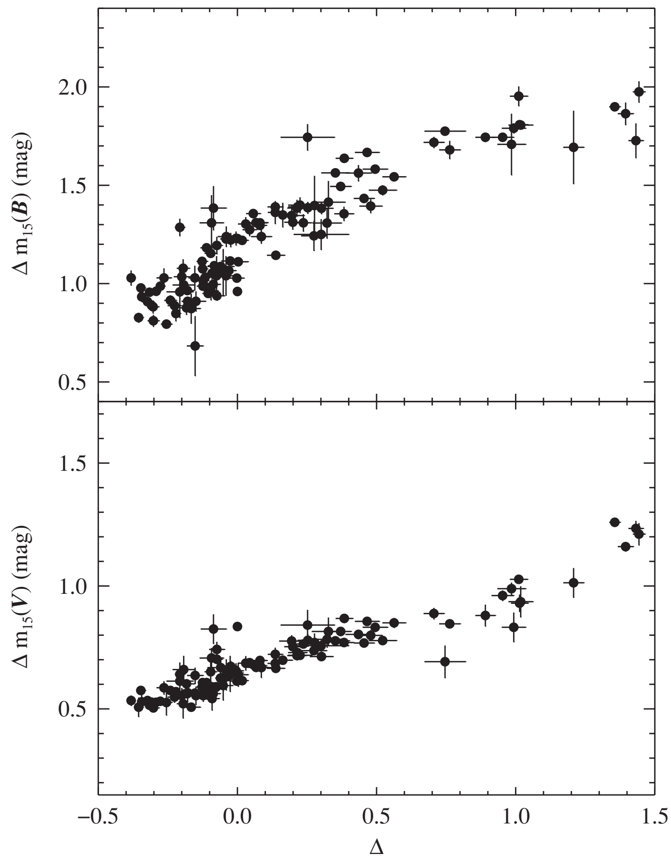

Figure 28. Comparisons of Δ to $\Delta m_{15}(B)$ and $\Delta m_{15}(V)$. Both Δ and Δm_{15} are measurements that correlate light-curve shape with intrinsic luminosity. A linear correlation holds for most of the SNe in the sample. Fast declining SNe ($\Delta \gtrsim 0.8$) do not seem to follow the trend set by rest of the sample.

the number of SNe found as a function of galaxy morphology for the three sets of SNe. We caution the reader from drawing extensive conclusions from this figure, as our sample may suffer from significant observational biases. However, it is interesting to note that our sample follows many relationships that have been previously noticed. Fast decliners in our sample are more likely to be found in early-type galaxies, while normal and slow decliners seem to favor later types (Della Valle & Livio 1994; Hamuy et al. 1996b; Howell 2001). While it is tempting to conclude that more than one population of stars gives rise to SNe Ia, the observational bias in our photometric data set must be kept in mind.

5.4. Δ and Δm_{15}

We compare Δ with our direct fits to $\Delta m_{15}(B)$ and $\Delta m_{15}(V)$ in Figure 28. As both are a proxy for the absolute magnitude of an SN, there is clearly a trend between the two. In both plots, the fastest decliners ($\Delta \geqslant 0.75$) do not seem to lie on the linear trend set by the rest of the sample.

6. CONCLUSION

We have presented *BVRI* light curves of 165 SNe Ia, most of which are of high quality and well sampled. This represents a homogeneously observed and reduced data set. We estimate the systematic error in our photometry data set to be 0.03 mag in *BVRI*.

As a consistency check on our reduction procedure, we compared our results with previous manual reductions of LOSS data and with data from other telescopes. We find that in general there is very good agreement between the results presented here and those already in the literature.

A major goal in SN Ia photometry must be to understand the systematics that arise from combining large data sets. We have shown that by analyzing the overlapping CfA3 and LOSS photometry as a single ensemble, the average residual is within 0.02 mag in *BVRI*. However, the scatter is surprisingly large ($\sigma \approx 0.1$ mag). If we limit our analysis to overlapping points brighter than mag 18, we can reduce the scatter to within 0.06–0.07 mag, which is still quite high. This scatter is due to systematic offsets in individual SN data sets and could be the result of calibration differences or galaxy-subtraction inconsistencies.

We have measured various light-curve parameters for our data set that are useful in characterizing the light-curve shape versus luminosity relationship, including $\Delta m_{15}(B)$ and $\Delta m_{15}(V)$. We have also run MLCS2k2 on our data set, setting $R_V = 3.1$ to determine the parameter Δ. Our upcoming cosmology paper will use this data set to add to the existing literature on SN Ia cosmology. In particular, comparisons of MLCS2k2 with other distance fitters such as SALT, SALT2 (Guy et al. 2007), and a simple two-parameter fit will be used to attempt to disentangle the best method for handling reddening and for determining distances to SNe.

Understanding the effects of reddening is necessary in order to derive reliable distances to SNe Ia using distance fitters. We measured the distribution of $(B-V)_{35}$ for 76 SNe in our sample by fitting the late-time colors with the Lira–Phillips slope. Fitting the distribution with a normally distributed component modeling Gaussian variations in SN color convolved with a decaying exponential host-galaxy component, we found that the results are consistent with the priors used by MLCS2k2 at the

1σ level. Future studies will examine the validity of assuming a decaying exponential as the probability distribution function of galactic reddening and the observational bias included in our sample.

The true potential of our extensive photometric data set will be realized when analyzed in conjunction with the Berkeley Supernova Ia Program (BSNIP) spectroscopic database. We have ∼1400 spectra of ∼600 objects to be published soon (J. M. Silverman et al. 2010, in preparation). The overlap with the photometry is ∼120 objects with a median of three spectra per object. A detailed analysis combining our spectra with derived parameters from our photometry, such as Δ and Δm_{15}, is currently underway (J. M. Silverman et al. 2010, in preparation).

The future of SN Ia science remains promising. In combination with other large low-redshift data sets being released by the CfA and the CSP, the extensive sample of light curves will push studies of SN Ia cosmology to the limit of our understanding of these objects as distance indicators. The next step will be to combine the new nearby SN Ia data sets by accounting for *S*-corrections, putting all of the data sets on the same photometric system. This will require a vigilant comparison between the intersection of published data sets to understand systematic differences.

The research of A.V.F.'s supernova group at UC Berkeley has been generously supported by the US National Science Foundation (most recently through grants AST–0607485 and AST-0908886), the TABASGO Foundation, and Department of Energy grant DE-FG02-08ER41563. KAIT and its ongoing operation were made possible by donations from Sun Microsystems, Inc., the Hewlett-Packard Company, AutoScope Corporation, Lick Observatory, the NSF, the University of California, the Sylvia & Jim Katzman Foundation, and the TABASGO Foundation. We give particular thanks to Russ Genet, who made KAIT possible with his initial special gift; to Joseph S. Miller, then Director of Lick Observatory, who allowed A.V.F. to establish KAIT there; and to the TABASGO Foundation, without which this work would not have been completed. M.G. thanks N. McConnell, A. Miller, D. Poznanski, K. Shapiro, and X. Wang for many useful discussions. The very thoughtful and helpful comments provided by our referee, Alex Conley, substantially elevated the quality of this paper. We are grateful to the staff at Lick Observatory for assistance with KAIT and the Nickel telescope, and especially for making the Nickel remotely operable from campuses of the University of California. We made use of the NASA/IPAC Extragalactic Database (NED), which is operated by the Jet Propulsion Laboratory, California Institute of Technology, under contract with NASA.

Facilities: Nickel, KAIT

REFERENCES

Alard, C., & Lupton, R. H. 1998, ApJ, 503, 325
Aldering, G., et al. 2002, Proc. SPIE, 4836, 61
Anupama, G. C., Sahu, D. K., & Jose, J. 2005, A&A, 429, 667
Bessell, M. S. 1990, PASP, 102, 1181
Blondin, S., & Tonry, J. L. 2007, ApJ, 666, 1024
Boisseau, J. R., & Wheeler, J. C. 1991, AJ, 101, 1281
Chevalier, C., & Ilovaisky, S. A. 1991, A&AS, 90, 225
Contreras, C., et al. 2010, AJ, 139, 519
Della Valle, M., & Livio, M. 1994, ApJ, 423, L31
Filippenko, A. V. 1997, ARA&A, 35, 309
Filippenko, A. V. 2003, in From Twilight to Highlight: The Physics of Supernovae, ed. W. Hillebrandt & B. Leibundgut (New York: Springer-Verlag), 171
Filippenko, A. V. 2005a, in ASP Conf. Ser. 342, 1604-2004: Supernovae as Cosmological Lighthouses, ed. M. Turatto et al. (San Francisco, CA: ASP), 87
Filippenko, A. V. 2005b, in Astrophysics and Space Science Library, Vol. 332, White Dwarfs: Cosmological and Galactic Probes, ed. E. M. Sion, S. Vennes, & H. L. Shipman (Dordrecht: Springer), 97
Filippenko, A. V., Li, W. D., Treffers, R. R., & Modjaz, M. 2001, in ASP Conf. Ser. 246, IAU Colloq. 183: Small Telescope Astronomy on Global Scales, ed. B. Paczynski, W.-P. Chen, & C. Lemme (San Francisco, CA: ASP), 121
Filippenko, A. V., et al. 1992a, AJ, 104, 1543
Filippenko, A. V., et al. 1992b, ApJ, 384, L15
Folatelli, G., et al. 2010, AJ, 139, 120
Garnavich, P. M., et al. 2004, ApJ, 613, 1120
Guy, J., et al. 2007, A&A, 466, 11
Hamuy, M., Phillips, M. M., Suntzeff, N. B., Schommer, R. A., Maza, J., & Aviles, R. 1996a, AJ, 112, 2391
Hamuy, M., Phillips, M. M., Suntzeff, N. B., Schommer, R. A., Maza, J., & Aviles, R. 1996b, AJ, 112, 2398
Hamuy, M., Phillips, M. M., Suntzeff, N. B., Schommer, R. A., Maza, J., Smith, R. C., Lira, P., & Aviles, R. 1996c, AJ, 112, 2438
Hamuy, M., et al. 1996d, AJ, 112, 2408
Hicken, M., Wood-Vasey, W. M., Blondin, S., Challis, P., Jha, S., Kelly, P. L., Rest, A., & Kirshner, R. P. 2009a, ApJ, 700, 1097
Hicken, M., et al. 2009b, ApJ, 700, 331
Howell, D. A. 2001, ApJ, 554, L193
Jha, S., Branch, D., Chornock, R., Foley, R. J., Li, W., Swift, B. J., Casebeer, D., & Filippenko, A. V. 2006a, AJ, 132, 189
Jha, S., Riess, A. G., & Kirshner, R. P. 2007, ApJ, 659, 122
Jha, S., et al. 2006b, AJ, 131, 527
Kowalski, M., et al. 2008, ApJ, 686, 749
Krajnović, D., Cappellari, M., de Zeeuw, P. T., & Copin, Y. 2006, MNRAS, 366, 787
Krisciunas, K., Hastings, N. C., Loomis, K., McMillan, R., Rest, A., Riess, A. G., & Stubbs, C. 2000, ApJ, 539, 658
Krisciunas, K., et al. 2004, AJ, 128, 3034
Landolt, A. U. 1983, AJ, 88, 439
Landolt, A. U. 1992, AJ, 104, 340
Leibundgut, B., et al. 1993, AJ, 105, 301
Leloudas, G., et al. 2009, A&A, 505, 265
Leonard, D. C., Li, W., Filippenko, A. V., Foley, R. J., & Chornock, R. 2005, ApJ, 632, 450
Li, W., Filippenko, A. V., Chornock, R., & Jha, S. 2003a, PASP, 115, 844
Li, W., Filippenko, A. V., & Riess, A. G. 2001a, ApJ, 546, 719
Li, W., Filippenko, A. V., Treffers, R. R., Riess, A. G., Hu, J., & Qiu, Y. 2001b, ApJ, 546, 734
Li, W. D., et al. 2000, in AIP Conf. Ser. 522, Cosmic Explosions: Tenth Astrophysics Conference, ed. S. S. Holt & W. W. Zhang (Melville, NY: AIP), 103
Li, W., et al. 2001c, PASP, 113, 1178
Li, W., et al. 2003b, PASP, 115, 453
Li, W., et al. 2010, MNRAS, submitted (arXiv:1005.4612)
Lira, P. 1996, Master's thesis, Univ. Chile
Miller, J. S., & Stone, R. P. S. 1993, Lick Obs. Tech. Rep. 66 (Santa Cruz, CA: Lick Obs.)
Modjaz, M., Li, W., Filippenko, A. V., King, J. Y., Leonard, D. C., Matheson, T., Treffers, R. R., & Riess, A. G. 2001, PASP, 113, 308
Pastorello, A., et al. 2007, MNRAS, 377, 1531
Perlmutter, S., et al. 1997, ApJ, 483, 565
Perlmutter, S., et al. 1999, ApJ, 517, 565
Phillips, A. C., & Davis, L. E. 1995, in ASP Conf. Ser. 77, Astronomical Data Analysis Software and Systems IV, ed. R. A. Shaw, H. E. Payne, & J. J. E. Hayes (San Francisco, CA: ASP), 297
Phillips, M. M. 1993, ApJ, 413, L105
Phillips, M. M., Lira, P., Suntzeff, N. B., Schommer, R. A., Hamuy, M., & Maza, J. 1999, AJ, 118, 1766
Phillips, M. M., Wells, L. A., Suntzeff, N. B., Hamuy, M., Leibundgut, B., Kirshner, R. P., & Foltz, C. B. 1992, AJ, 103, 1632
Phillips, M. M., et al. 2007, PASP, 119, 360
Poznanski, D., et al. 2009, ApJ, 694, 1067
Prieto, J. L., Rest, A., & Suntzeff, N. B. 2006, ApJ, 647, 501
Richmond, M., Treffers, R. R., & Filippenko, A. V. 1993, PASP, 105, 1164
Riess, A. G., Press, W. H., & Kirshner, R. P. 1995, ApJ, 438, L17
Riess, A. G., Press, W. H., & Kirshner, R. P. 1996, ApJ, 473, 88
Riess, A. G., et al. 1998, AJ, 116, 1009
Riess, A. G., et al. 1999, AJ, 117, 707

Riess, A. G., et al. 2007, ApJ, 659, 98
Riess, A. G., et al. 2009, ApJS, 183, 109
Schlegel, D. J., Finkbeiner, D. P., & Davis, M. 1998, ApJ, 500, 525
Schmidt, B. P., et al. 1998, ApJ, 507, 46
Stanishev, V., et al. 2007, A&A, 469, 645
Stetson, P. B. 1987, PASP, 99, 191
Stritzinger, M., Suntzeff, N. B., Hamuy, M., Challis, P., Demarco, R., Germany, L., & Soderberg, A. M. 2005, PASP, 117, 810
Stritzinger, M., et al. 2002, AJ, 124, 2100
Wang, X., et al. 2009a, ApJ, 699, L139
Wang, X., et al. 2009b, ApJ, 697, 380
Wood-Vasey, W. M., et al. 2007, ApJ, 666, 694